Research Square

Preprints are preliminary reports that have not undergone peer review.
They should not be considered conclusive, used to inform clinical practice,
or referenced by the media as validated information.

Copper- and Chromium-Exchanged Faujasite Zeolites: Structure, Acidity and Catalytic Performance in Ethanol Conversion

Asmer Valiyeva

sdtksdu@gmail.com

Azerbaijan State Oil and Industry University

Jabrail Mirzai

Baku State University

Mahira Aliyeva

Azerbaijan State Oil and Industry University

Mehriban Mikayilova

Azerbaijan State Oil and Industry University

Sadaqat Ibrahimova

Azerbaijan State Oil and Industry University

Tunzala Majidova

Sumgayit State Technical College under Sumgayit State University

Research Article

Keywords: FAU zeolite, ethanol conversion, ethylene, acetaldehyde, Lewis acidity, catalytic stability

Posted Date: November 18th, 2026

DOI: https://doi.org/10.21203/rs.3.rs-10939556/v1

License: This work is licensed under a Creative Commons Attribution 4.0 International License.
Read Full License

Additional Declarations: No competing interests reported.

COPPER- AND CHROMIUM-EXCHANGED FAUJASITE ZEOLITES: STRUCTURE, ACIDITY AND CATALYTIC PERFORMANCE IN ETHANOL CONVERSION

Asmer Valiyeva[1*], Jabrail Mirzai[2], Mahira Aliyeva[1], Mehriban Mikayilova[1], Sadaqat Ibrahimova[1], Tunzala Majidova[3]

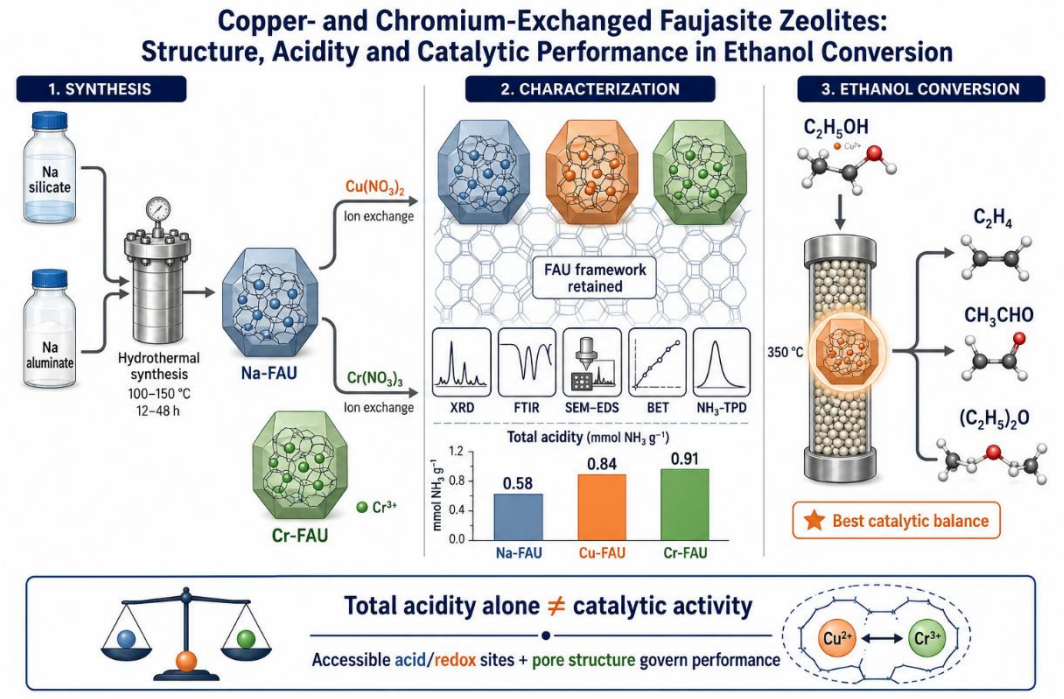
[1]Department of Chemical Engineering, Azerbaijan State Oil and Industry University, 20 Azadliq Avenue, Baku AZ1010, Azerbaijan

[2]Department of Chemistry, Baku State University, 23 Zahid Khalilov Street, Baku AZ1148, Azerbaijan

[3] Sumgayit State Technical College under Sumgayit State University, Heydar Aliyev Ave.37, Sumgayit AZ5000, Azerbaijan

Highlights

- Transition-metal ion exchange effectively tailored the acidity of FAU zeolites.
- The FAU crystalline framework retained its structural integrity after Cu^{2+} and Cr^{3+} ion exchange.
- Cu-FAU exhibited high catalytic activity for ethanol dehydration towards ethylene formation.
- Cr-FAU promoted the selective dehydrogenation of ethanol to acetaldehyde.
- The structure–acidity–catalytic performance relationship was established for FAU-based catalysts.



Abstract

Cu- and Cr-exchanged faujasite catalysts were prepared by successive ion exchange of hydrothermally synthesised Na-FAU and evaluated for gas-phase ethanol conversion. The effects of metal exchange on the structure, porosity, acidity and catalytic behaviour of the FAU zeolite were investigated using PXRD, XRF, ICP-OES, SEM–EDS, N_2 physisorption, FTIR, Py-FTIR, ^{27}Al and ^{29}Si MAS NMR, NH_3-TPD and TGA/DTG. The FAU framework and characteristic crystal morphology were largely retained after Cu^{2+} and Cr^{3+} exchange, while no separate crystalline CuO or Cr_2O_3 phases were detected. The degrees of ion exchange were 74% for Cu-FAU and 42% for Cr-FAU. Metal incorporation moderately reduced the BET surface area from 721 $m^2\ g^{-1}$ for Na-FAU to 654 and 628 $m^2\ g^{-1}$ for Cu-FAU and Cr-FAU, respectively, without destroying the predominantly microporous structure. Py-FTIR showed that Cu exchange produced the largest relative increase in Lewis acidity, whereas NH_3-TPD indicated total acidities of 0.58, 0.84 and 0.91 mmol $NH_3\ g^{-1}$ for Na-FAU, Cu-FAU and Cr-FAU, respectively. At 350 °C, ethanol conversion reached 62% over Na-FAU, 91% over Cu-FAU and 79% over Cr-FAU. Cu-FAU favoured ethanol dehydration, providing 76% ethylene selectivity and a 69.2% ethylene yield. In contrast, Cr-FAU favoured dehydrogenation, achieving 63% acetaldehyde selectivity and a 49.8% yield. Cu-FAU also exhibited the highest stability, retaining 88% conversion after 24 hours and 95.6% of its initial activity after five reaction–regeneration cycles. These results demonstrate that ethanol conversion over metal-exchanged FAU catalysts is governed by the combined effects of metal-cation identity, acid-site nature and strength, degree of ion exchange and pore accessibility rather than by total acidity or surface area alone.
Keywords: FAU zeolite; ethanol conversion; ethylene; acetaldehyde; Lewis acidity; catalytic stability

1. Introduction

Bioethanol derived from renewable feedstocks is a promising platform molecule for producing high-value products such as ethylene, acetaldehyde, diethyl ether and 1,3-butadiene. The catalytic conversion pathway of ethanol depends on the acid–base and redox properties of the catalyst, its pore structure, the accessibility of its active sites and the reaction conditions. Intramolecular dehydration of ethanol over acid sites predominantly produces ethylene, whereas intermolecular dehydration leads to the formation of diethyl ether. Metal and metal oxide sites may promote the dehydrogenation of ethanol to acetaldehyde [1-2]. Therefore, establishing an appropriate balance between the acid and redox sites of the catalyst is essential for achieving both high conversion and selectivity towards the desired product.

γ-Al_2O_3, heteropolyacids, silica–alumina oxides and various zeolites have been used for the dehydration of bioethanol to ethylene. Zeolites differ from other solid acid catalysts because of their high specific surface area, ordered pore structure, tuneable acidity and ion-exchange capacity [3]. Wu and Wu (2017) [4] demonstrated that the dealumination of ZSM-5 altered its pore structure and acid-site distribution, resulting in high ethylene yield and selectivity at low temperatures. However, ethanol conversion is not determined solely by the total number of acid sites. Brønsted and Lewis acid sites perform different functions in the adsorption and activation of ethanol. Surface ethoxy species may form at Brønsted acid sites, whereas coordinated ethanol may form at Lewis acid sites, and the subsequent conversion of these intermediates influences the product distribution [5-6].

FAU-type zeolites possess a three-dimensional channel system, wide pore openings, large supercages and a high cation-exchange capacity, making their structure suitable for catalytic applications. The substitution of Si atoms by Al atoms within the FAU framework generates a negative charge, which is compensated by exchangeable cations located within the pores. Replacing Na^+ ions with transition-metal cations enables the acidity, redox properties and adsorption capacity of the zeolite to be modified in a controlled manner [7]. At the same time, ion exchange may affect the location of metal species within the pores, the specific surface area, the micropore volume and the accessibility of active sites. Excessive metal loading may result in partial pore blockage and the formation of metal oxide aggregates [8].

In Cu-exchanged zeolites, ionic and highly dispersed Cu species provide active sites for alcohol dehydrogenation. Yu et al. (2019) [9] found that Cu species stabilised within the zeolite exhibited high activity in the conversion of ethanol to acetaldehyde. Nevertheless, the reduction of CuO species to Cu^+ and Cu^0 during the reaction, followed by sintering, may lead to catalyst deactivation. The catalytic effect of Cu species depends not only on their total amount but also on their oxidation state, dispersion and location relative to the acid sites [10-11]. Therefore, the interaction between the metal centres and the acid sites of the zeolite in a Cu-FAU catalyst may play an important role in determining selectivity towards ethylene, acetaldehyde and diethyl ether.

In Cr-exchanged zeolites, chromium species with different oxidation and coordination states may generate Lewis acid and redox sites. Ayari et al. (2012) [12] demonstrated that the chemical state and catalytic accessibility of Cr species depended strongly on the zeolite topology. Although chromate and polychromate species, oxo cations and small Cr_2O_3 clusters may be active in catalytic processes, large Cr_2O_3 aggregates can block the pores and reduce the accessibility of active sites. In metal–zeolite systems, catalytic behaviour is shaped by the interaction of the metal centre with the zeolite framework and neighbouring oxygen atoms. Therefore, in addition to the type of metal, its location within the zeolite microenvironment and its coordination structure must also be considered [13].

In the literature, ethanol dehydration has primarily been investigated over ZSM-5 and other medium-pore zeolites. A substantial proportion of studies on Cu-based systems have focused on methane oxidation, whereas research on Cr-containing zeolites has mainly addressed hydrocarbon dehydrogenation and ammoxidation [14-15]. By comparison, studies that comparatively investigate the relationship between the structural, textural and acidic properties of Na-, Cu- and Cr-forms prepared from the same FAU matrix and their catalytic behaviour in ethanol conversion remain limited.

In this study, Na-FAU zeolite was synthesised and subsequently exchanged with Cu^{2+} and Cr^{3+} ions to prepare Cu-FAU and Cr-FAU catalysts. The study aimed to determine the effects of metal-ion exchange on the crystal structure, morphology, elemental composition, pore characteristics and acid-

site distribution of FAU zeolite, as well as to compare the activity and product selectivity of Na-FAU, Cu-FAU and Cr-FAU samples in ethanol conversion. This approach may help clarify the relationship between the nature of the metal cation and the structure–acidity–activity correlation, thereby providing a scientific basis for developing FAU-based catalysts for the selective conversion of bioethanol.

2. Literature Review

2.1. Structure and Synthesis Characteristics of FAU-Type Zeolites

FAU-type zeolites have a three-dimensional crystalline structure composed of SiO_4 and AlO_4 tetrahedra. Their structure contains sodalite cages, hexagonal prisms and supercages approximately 1.3 nm in size. Access to the supercages is provided through 12-membered oxygen rings with an opening of approximately 0.74 nm. The wide pore system facilitates reactant diffusion, the accommodation of exchangeable cations and the formation of catalytic sites. The negative charge generated by the substitution of Si^{4+} ions with Al^{3+} in the framework is compensated by Na^+ and other exchangeable cations. This property makes FAU zeolites suitable supports for the incorporation of metal ions [16, 17].

The phase purity of NaX-type FAU zeolite depends on the temperature and duration of hydrothermal synthesis, the degree of alkalinity, the ageing stage and the Si/Al ratio of the initial gel. Ahmadon et al. (2018) [18] demonstrated that hydrothermal treatment at 90 °C for 16 hours enabled the formation of a pure NaX phase with high crystallinity. The formation of secondary phases such as NaP was observed at longer crystallisation times. Guan et al. (2019) [19] found that alkalinity, temperature and hydrothermal treatment time must be maintained at optimum levels for the formation of FAU crystals. Excessive alkalinity and temperature may lead to the dissolution of FAU crystals and the formation of the more stable sodalite phase. These findings indicate that preparing a highly crystalline, phase-pure Na-FAU support is a fundamental requirement before metal ion exchange.

2.2. Effect of Cu and Cr Ion Exchange on the FAU Structure

Ion exchange involves replacing the original Na^+ cations of the FAU zeolite with transition-metal ions such as Cu^{2+} and Cr^{3+}. During this process, the metal cations may occupy sites within the supercages and sodalite cages or near the six-membered rings. The charge and ionic radius of the metal, its degree of hydration and the distribution of Al within the zeolite determine the exchange sites. Changing the charge-compensating cation affects the pore volume, specific surface area, water adsorption and local framework structure [20, 21].

In Cu-exchanged zeolites, catalytic activity depends more strongly on the dispersion and coordination state of the Cu species than on the total metal content. Kvande et al. (2023) [8] found that a high

Cu/Al ratio led to an uneven metal distribution, the formation of Cu aggregates and partial pore blockage. Wang et al. (2018) showed that isolated ionic Cu species in Cu-zeolites were more active than large CuO particles. The distance between Cu centres and acid sites also affects the conversion of intermediate compounds and product selectivity [22]. Under reaction conditions, the migration, reduction and aggregation of Cu species may lead to catalyst deactivation [10].

In Cr-exchanged zeolites, chromium may be present as isolated Cr cations, oxo cations, chromate and polychromate species, as well as Cr_2O_3 clusters. Ayari et al. (2012) [12] demonstrated that chromium speciation depended strongly on the zeolite topology. Although small and well-dispersed Cr oxide species are catalytically favourable, large Cr_2O_3 aggregates restrict access to the pores. Within the FAU structure, some Cr species located in the sodalite and hexagonal cages may remain inaccessible to reactants. The coordination state of Cr^{3+} species and their interaction with the support determine their dehydrogenation and redox activity [23, 24].

2.3. Metal Exchange, Acidity and Catalytically Active Sites

The catalytic activity of zeolites is related to the concentration, strength and accessibility of their Brønsted and Lewis acid sites. Brønsted acidity mainly originates from bridging Si–OH–Al hydroxyl groups, whereas Lewis acidity arises from extra-framework Al species, coordinatively unsaturated metal cations and structural defects. Jiao et al. (2005) [25] showed that framework and extra-framework Al species in FAU-type Y zeolite existed in different coordination states. Batool et al. (2022) [26] established a quantitative relationship between the amount of extra-framework Al, the concentration of Lewis acid sites and catalytic activity.

Metal ion exchange may alter the acidity of Na-FAU in two main ways. First, Cu and Cr cations create Lewis acid sites that accept electron pairs. Second, ion exchange and subsequent thermal treatment may alter the local environment of framework Al, leading to the formation of new hydroxyl groups and extra-framework species. At the same time, the formation of metal oxide aggregates may cover some of the acid sites and restrict the access of reactants to the pores. Therefore, both the total acidity and its distribution among weak, medium-strength and strong sites should be evaluated.

NH_3-TPD is widely used to determine the total concentration and strength distribution of acid sites. Desorption observed at low temperatures is generally associated with weak acid sites, whereas desorption at higher temperatures is attributed to stronger acid sites [27]. However, additional techniques, such as pyridine-FTIR or solid-state NMR, are required to distinguish between Brønsted and Lewis acid sites [28, 29]. Therefore, the combined analysis of XRD, FTIR, SEM–EDS, N_2 adsorption–desorption and NH_3-TPD results provides a more reliable interpretation of the structural and acidic changes caused by metal exchange.

2.4. Product Selectivity in Ethanol Conversion and the Research Gap

The conversion of ethanol over zeolite catalysts involves parallel and consecutive reactions. Brønsted and Lewis acid sites promote ethanol dehydration, resulting in the formation of ethylene and diethyl ether. Relatively low temperatures and high surface coverage favour intermolecular dehydration and diethyl ether formation, whereas higher temperatures promote intramolecular dehydration and increase ethylene selectivity [3, 4]. Substrate concentration and the clustering of ethanol molecules within the pores may also affect the activation energy and reaction rate [30].

Surface ethoxy and oxonium species are regarded as key intermediates in ethanol dehydration. Zhou et al. (2019) [5] observed the triethyloxonium ion over H-ZSM-5 and showed that it formed part of the pathway leading to ethylene production. Hu et al. (2026) [6] found that Lewis acid sites readily activated the –OH group of ethanol at low temperatures, although the β-H elimination step encountered a higher kinetic barrier. At Brønsted acid sites, initial activation was relatively more difficult, but ethylene formation could proceed more readily.

The incorporation of Cu species may promote the dehydrogenation of ethanol to acetaldehyde alongside dehydration. Yu et al. (2019) [9] demonstrated that acetaldehyde was produced with a yield of approximately 70% and maintained stable performance for up to 100 hours over Beta zeolite modified with highly dispersed Cu species. Owing to their redox and Lewis acid properties, Cr centres may also participate in the activation of C–H and O–H bonds. However, information directly comparing FAU-based Cu- and Cr-exchanged catalysts in ethanol conversion remains limited.

Thus, although FAU synthesis, Cu and Cr speciation, zeolite acidity and ethanol conversion have each been extensively investigated, the systematic relationship between the structural and acidic changes caused by Cu^{2+} and Cr^{3+} exchange within the same Na-FAU support and the resulting product selectivity has not been sufficiently clarified. The present study aims to address this gap by evaluating the crystal structure, porosity, elemental distribution, acid sites and catalytic performance of Na-FAU, Cu-FAU and Cr-FAU samples in ethanol conversion using a unified comparative approach.

3. Experimental Section

3.1. Materials

Sodium silicate solution (Na_2SiO_3, 26–28 wt% SiO_2), sodium aluminate ($NaAlO_2$, 50–56 wt% Al_2O_3), copper(II) nitrate trihydrate ($Cu(NO_3)_2 \cdot 3H_2O$, ≥99.9%) and chromium(III) nitrate nonahydrate ($Cr(NO_3)_3 \cdot 9H_2O$, ≥99.9%) were obtained from Sigma-Aldrich (St. Louis, MO, USA). Sodium silicate and sodium aluminate were used as the silicon and aluminium sources, respectively, whereas the copper(II) and chromium(III) nitrate salts were used as ion-exchange precursors.

Ethanol was used as the reactant in the catalytic conversion tests, whereas pyridine was employed as a probe molecule to identify Brønsted and Lewis acid sites by FTIR spectroscopy. A mixture

containing 10 vol% NH_3 in helium was used for the NH_3-TPD measurements, while helium and nitrogen were used for sample pretreatment and catalytic testing, respectively. Inert quartz particles were used to dilute the reactor bed. During gas chromatographic analysis, the reaction components were identified and quantified using authentic standards. All reagents were used as supplied without further purification. Deionised water was used to prepare the synthesis gel and analytical solutions and during the ion-exchange and sample-washing stages.

3.2. Synthesis of Na-FAU Zeolite

Na-FAU zeolite was synthesised by alkaline hydrothermal crystallisation. The initial gel was prepared with a molar composition of 3.0 Na_2O : Al_2O_3 : 6.0 SiO_2 : 200 H_2O. Sodium aluminate was dissolved in deionised water, after which the sodium silicate solution was gradually added to the resulting solution. The mixture was continuously stirred until a homogeneous gel formed and was aged at room temperature for 24 hours before crystallisation.

The aged synthesis gel was transferred to a Teflon-lined stainless-steel autoclave and subjected to hydrothermal treatment under static conditions at 100 °C for 48 hours. After crystallisation, the autoclave was cooled to room temperature, and the resulting solid product was separated from the liquid phase by vacuum filtration. The product was repeatedly washed with deionised water until the pH of the filtrate approached neutrality and was then dried overnight at 110 °C.

The dried sample was heated to 550 °C in an air atmosphere at a heating rate of 5 °C min^{-1} and maintained at this temperature for 5 hours. The resulting zeolite sample was designated Na-FAU for subsequent ion-exchange and characterisation procedures.

3.3. Preparation of Cu-FAU and Cr-FAU Catalysts

The Cu-FAU and Cr-FAU catalysts were prepared by modifying the synthesised Na-FAU zeolite through successive ion-exchange treatments in an aqueous medium. In each ion-exchange experiment, 2.0 g of the Na-FAU sample was dispersed in 200 mL of metal nitrate solution. A 0.10 mol L^{-1} $Cu(NO_3)_2$ solution was used for copper exchange, whereas a 0.05 mol L^{-1} $Cr(NO_3)_3$ solution was used for chromium exchange. The resulting suspensions were maintained at 80 °C for 24 hours under stirring at 500 rpm.

After the first exchange stage, the solid phase was separated by vacuum filtration and washed with deionised water until the soluble residual species had been removed. To increase the degree of metal-ion incorporation into the zeolite, the same procedure was repeated twice using freshly prepared precursor solutions. Thus, each sample underwent a total of three successive ion-exchange cycles.

Following the final exchange stage, the samples were separated by vacuum filtration, washed with deionised water and dried overnight at 110 °C. The dried materials were heated to 500 °C under

flowing air at a heating rate of 5 °C min^{-1} and calcined at this temperature for 4 hours. The copper- and chromium-modified samples were designated Cu-FAU and Cr-FAU, respectively.

The degree of ion exchange was calculated from the metal content determined by ICP-OES and the sodium content of the original Na-FAU sample, taking charge equivalence into account:

$$IE_{\mathrm{metal}}(\%) = \frac{n_{\mathrm{metal}} z_{\mathrm{metal}}}{n_{\mathrm{Na}} z_{\mathrm{Na}}} \times 100$$

where IE_{metal} is the degree of ion exchange for the metal, n_{metal} is the amount of Cu or Cr incorporated into the zeolite (mmol g^{-1}), n_{Na} is the sodium content of the original Na-FAU sample (5.17 mmol g^{-1}), z_{metal} is the charge of the incorporated metal cation and z_{Na} is the charge of the Na^+ ion. Values of $z_{\mathrm{metal}} = 2$for Cu^{2+}, $z_{\mathrm{metal}} = 3$for Cr^{3+} and $z_{\mathrm{Na}} = 1$for Na^+ were used in the calculations.

3.4. Characterisation Methods

The phase composition and crystal structure of the Na-FAU, Cu-FAU and Cr-FAU samples were examined by powder X-ray diffraction (PXRD). The diffraction patterns were recorded using Cu Kα radiation. The phases were identified by comparing the experimental diffraction reflections with standard data for the FAU topology. The relative crystallinity of the samples was calculated from the sum of the integrated areas of the five most intense FAU reflections, with the crystallinity of Na-FAU taken as 100%:

$$\text{Relative crystallinity (\%)} = \frac{\sum A_{\mathrm{sample}}}{\sum A_{\text{Na-FAU}}} \times 100$$

where Arepresents the integrated area of the selected FAU reflections after background correction.

The textural properties of the samples were determined by nitrogen adsorption–desorption measurements at −196 °C using a Micromeritics ASAP 2020 analyser. Before measurement, the samples were degassed under vacuum at 300 °C for 3 hours. The specific surface area was calculated using the Brunauer–Emmett–Teller (BET) model. The micropore area and micropore volume were determined using the t-plot method, while the total pore volume was estimated from the amount of nitrogen adsorbed in the saturation region of the isotherm. The mesopore size distribution was analysed by applying the Barrett–Joyner–Halenda (BJH) model to the desorption branch of the isotherm.

The particle morphology and crystal size of the samples were examined using a Carl Zeiss Supra 40VP field-emission scanning electron microscope equipped with an Oxford X-Max 80 energy-dispersive X-ray detector. The spatial distributions of Si, Al, Na, Cu and Cr in the Cu-FAU and Cr-FAU samples were evaluated by SEM–EDS elemental mapping. EDS spectra and elemental maps

were recorded from different areas of each sample to examine local variations in elemental composition and the homogeneity of the metal distribution.

Conventional FTIR spectra were recorded using the KBr disc method on a Bruker TENSOR 27 spectrometer over the wavenumber range of 400–4000 cm^{-1} at a spectral resolution of 4 cm^{-1}. Brønsted and Lewis acid sites on the zeolite surfaces were distinguished using pyridine-adsorbed FTIR spectroscopy. For this purpose, the samples were prepared as self-supporting discs with a surface density of 10 mg cm^{-2}, activated under vacuum at 450 °C for 1 hour and exposed to pyridine vapour at 150 °C. After weakly and physically adsorbed pyridine had been removed under vacuum, the spectra were recorded following evacuation at 200 and 350 °C. The bands observed at approximately 1545 and 1450 cm^{-1} were assigned to pyridine protonated at Brønsted acid sites and pyridine coordinated to Lewis acid sites, respectively. The integrated areas of the corresponding bands were determined using the same sample density and evacuation conditions and were normalised to the values obtained for Na-FAU before being presented as relative intensities.

The thermal behaviour of the samples was investigated by thermogravimetric analysis (TGA) using a NETZSCH TG 209 F3 Tarsus instrument. The measurements were performed under a nitrogen atmosphere over the temperature range of 30–800 °C at a heating rate of 10 °C min^{-1}. The mass-loss stages were evaluated through the combined analysis of the thermogravimetric and differential thermogravimetric curves.

The local coordination environments of the aluminium and silicon atoms were examined by solid-state ^{27}Al and ^{29}Si magic-angle-spinning nuclear magnetic resonance (MAS NMR) spectroscopy using a Bruker Avance III 400 MHz spectrometer. The ^{27}Al MAS NMR spectra were used to identify tetrahedral framework aluminium and possible extra-framework aluminium species, whereas the ^{29}Si MAS NMR spectra were used to assess the Q^n coordination environments of silicon.

The overall chemical composition of the samples was determined by X-ray fluorescence spectroscopy (XRF). Na, Cu and Cr contents were quantified by inductively coupled plasma–optical emission spectrometry (ICP-OES) following microwave-assisted acid digestion of the samples. The Si/Al ratio was calculated from the XRF results, while the Na, Cu and Cr contents measured by ICP-OES were used to determine the degree of ion exchange.

The total concentration and strength distribution of the acid sites were examined by ammonia temperature-programmed desorption (NH_3-TPD) using a Micromeritics AutoChem II 2920 analyser. Approximately 100 mg of each sample was pretreated under helium flow at 500 °C for 1 hour and then cooled to 100 °C before being saturated with a mixture containing 10 vol% NH_3 in helium. Physically and weakly adsorbed ammonia was removed by purging with helium. The desorption profiles were recorded over the temperature range of 100–600 °C at a heating rate of 10 °C min^{-1}. The total acid-site concentration was calculated from the integrated area of the NH_3 desorption signal,

while the contributions in the low- and high-temperature regions were analysed separately to assess the relative strength distribution of the acid sites.

3.5. Catalytic Tests

The catalytic activity of the Na-FAU, Cu-FAU and Cr-FAU samples was evaluated in the gas-phase conversion of ethanol. The experiments were conducted at atmospheric pressure in a fixed-bed tubular reactor made of stainless steel with an internal diameter of 10 mm. For each test, 0.30 g of catalyst with a particle size of 250–425 μm was used. To minimise heat- and mass-transfer limitations and improve temperature distribution within the catalyst bed, the catalyst was mixed with inert quartz particles at a mass ratio of 1:5.

Ethanol was introduced into the reactor using nitrogen as the carrier gas. The nitrogen stream was passed through an ethanol saturator maintained at 20 °C, and the partial pressure of ethanol in the gas mixture was maintained at 5.8 kPa. The nitrogen flow rate was 30 mL min^{-1}. A stable flow and saturation conditions were established before the ethanol-containing gas stream was introduced into the reactor.

Catalytic tests were conducted at 200, 250, 300, 350, 400 and 450 °C. At each temperature, the reaction was continued for 1 hour after the system had reached steady-state conditions, and the composition of the outlet stream was analysed by online gas chromatography. To ensure the comparability of the catalytic results, all samples were tested using the same catalyst mass, particle size, gas flow rate and ethanol partial pressure.

3.6. Product Analysis and Calculations

The reactor outlet stream was analysed online using an Agilent 7890B gas chromatograph equipped with an HP-PLOT/Q capillary column. Organic reaction components were detected using a flame ionisation detector (FID), whereas permanent gases were determined using a thermal conductivity detector (TCD). Ethanol and the products formed were identified by comparing their retention times with those of authentic standards. The components were quantified using calibration curves constructed from external standards for each compound.

Ethanol conversion was calculated from the molar flow rates of ethanol in the inlet and outlet streams using the following equation:

$$X_{\mathrm{EtOH}}(\%) = \frac{F_{\mathrm{EtOH,in}} - F_{\mathrm{EtOH,out}}}{F_{\mathrm{EtOH,in}}} \times 100$$

where $F_{\mathrm{EtOH,in}}$ and $F_{\mathrm{EtOH,out}}$ are the molar flow rates of ethanol entering and leaving the reactor, respectively.

The selectivity towards individual products was calculated on a carbon-molar basis:

$$S_i(\%) = \frac{n_{C,i} F_i}{\sum_j n_{C,j} F_j} \times 100$$

where F_i is the molar flow rate of product i, $n_{C,i}$ is the number of carbon atoms in one molecule of that product, and the sum in the denominator represents the total carbon-molar flow rate of all identified carbon-containing products. Unreacted ethanol was excluded from the selectivity calculation.

The product yield was determined from the ethanol conversion and the selectivity towards the corresponding product:

$$Y_i(\%) = \frac{X_{\mathrm{EtOH}} S_i}{100}$$

During the experiments, the carbon balance was calculated as the ratio of the total carbon-molar flow rate of the carbon-containing components identified at the reactor outlet to the carbon-molar flow rate of ethanol at the inlet:

$$CB(\%) = \frac{\sum_j n_{C,j} F_{j,\mathrm{out}}}{n_{C,\mathrm{EtOH}} F_{\mathrm{EtOH,in}}} \times 100$$

where CB is the carbon balance and $n_{C,\mathrm{EtOH}}$is the number of carbon atoms in an ethanol molecule. All conversion, selectivity and yield values were calculated from chromatographic data obtained after the system had reached steady-state conditions.

4. Results and Discussion

4.1. Crystal Structure and Phase Composition (PXRD)

Intense reflections were observed in the diffraction pattern of the Na-FAU sample and were assigned to the (111), (220), (311), (331), (333)/(511), (440), (533), (642) and (555)/(751) families of crystallographic planes, respectively. The agreement between the diffraction pattern presented in Figure 1 and the reference data for the FAU topology confirms that the faujasite structure was formed during hydrothermal synthesis [31, 32].

Following modification with Cu^{2+} and Cr^{3+} ions, the principal diffraction reflections of the FAU structure were retained in both the Cu-FAU and Cr-FAU samples. As shown in Figure 1, the ion-exchange and subsequent calcination stages did not produce any noticeable shifts or substantial broadening of the reflections. This observation indicates that metal modification did not significantly disrupt the long-range crystalline order of the FAU framework and that the aluminosilicate structure remained largely stable under the applied treatment conditions.

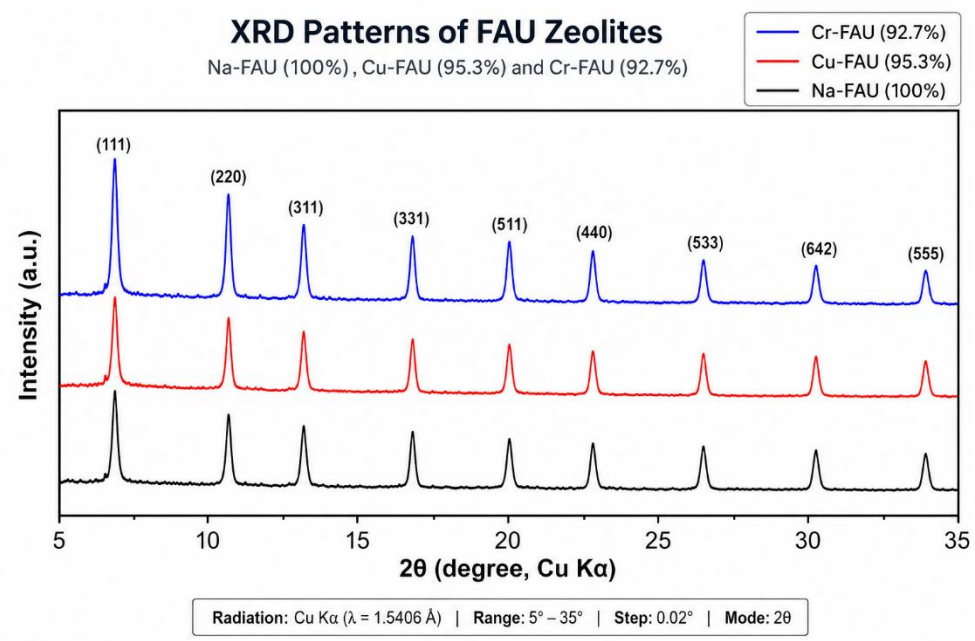


Figure 1. PXRD patterns of the Na-FAU, Cu-FAU and Cr-FAU samples recorded after ion exchange and calcination.

For the comparative assessment based on the integrated areas of the diffraction reflections, the crystallinity of the Na-FAU sample was taken as 100%. Using this approach, the relative crystallinities of the Cu-FAU and Cr-FAU samples were determined as 95.3% and 92.7%, respectively. The limited decrease observed in the metal-exchanged samples indicates that the repeated ion-exchange and thermal treatment stages had some effect on the crystalline order. Nevertheless, the complete retention of the principal FAU reflections confirms that these changes did not result in framework collapse or transformation into another crystalline zeolite phase.

Table 1. PXRD characteristics of the Na-FAU, Cu-FAU and Cr-FAU samples

Sample	**Relative crystallinity (%)**	**Principal crystalline phase**	**Secondary crystalline phase**	**Structural observation**
Na-FAU	100.0	FAU	Not detected	Intense and narrow FAU reflections
Cu-FAU	95.3	FAU	Not detected	FAU structure retained
Cr-FAU	92.7	FAU	Not detected	FAU structure retained, with a limited decrease in crystallinity

No distinct reflections attributable to crystalline CuO or Cr_2O_3 phases were observed in the diffraction patterns of the Cu-FAU and Cr-FAU samples. It can therefore be concluded that no large, highly crystalline metal oxide particles formed within the detection limit of PXRD. However, the absence of separate oxide reflections does not provide direct evidence that the Cu and Cr species were dispersed at the atomic level. The metal species may be present as ion-exchanged cations, small nanoclusters or X-ray-amorphous particles. Their amounts, distribution and chemical states should

therefore be evaluated together with the results of ICP-OES, XRF, SEM–EDS and appropriate spectroscopic analyses.

Overall, PXRD analysis shows that the faujasite phase was successfully formed in the Na-FAU sample and that the FAU topology was largely retained after ion exchange with Cu^{2+} and Cr^{3+}. The absence of secondary crystalline phases and the limited reduction in relative crystallinity demonstrate that the applied modification conditions were compatible with the zeolite framework. These findings provide a structural basis for the comparative interpretation of the chemical composition, textural properties, surface acidity and catalytic performance data presented in the following sections [33].

4.2. Chemical Composition and Degree of Ion Exchange (XRF/ICP-OES)

The overall chemical compositions of the Na-FAU, Cu-FAU and Cr-FAU samples were evaluated by XRF, while their sodium and transition-metal contents were determined by ICP-OES. The Si/Al molar ratios calculated from the XRF analysis were 2.50 for Na-FAU, 2.48 for Cu-FAU and 2.47 for Cr-FAU. The slight differences observed among the samples may be considered to fall within the variability of the analytical measurements. The fact that the Si/Al ratio remained largely unchanged after ion exchange indicates that the aqueous exchange and thermal treatment stages did not produce any noticeable change in the aluminosilicate composition. This result is consistent with the PXRD data presented in Section 4.1, which showed that the FAU topology was retained in all samples.

A substantial decrease in the sodium content of the samples was observed after ion exchange. The Na content decreased from 5.17 mmol g^{-1} in the original Na-FAU sample to 1.35 mmol g^{-1} in Cu-FAU and 3.00 mmol g^{-1} in Cr-FAU. This change indicates that the original Na^{+} ions were partially replaced by the corresponding metal cations. The oxide composition determined by XRF and the cation composition evaluated by ICP-OES are compared in Figure 2.

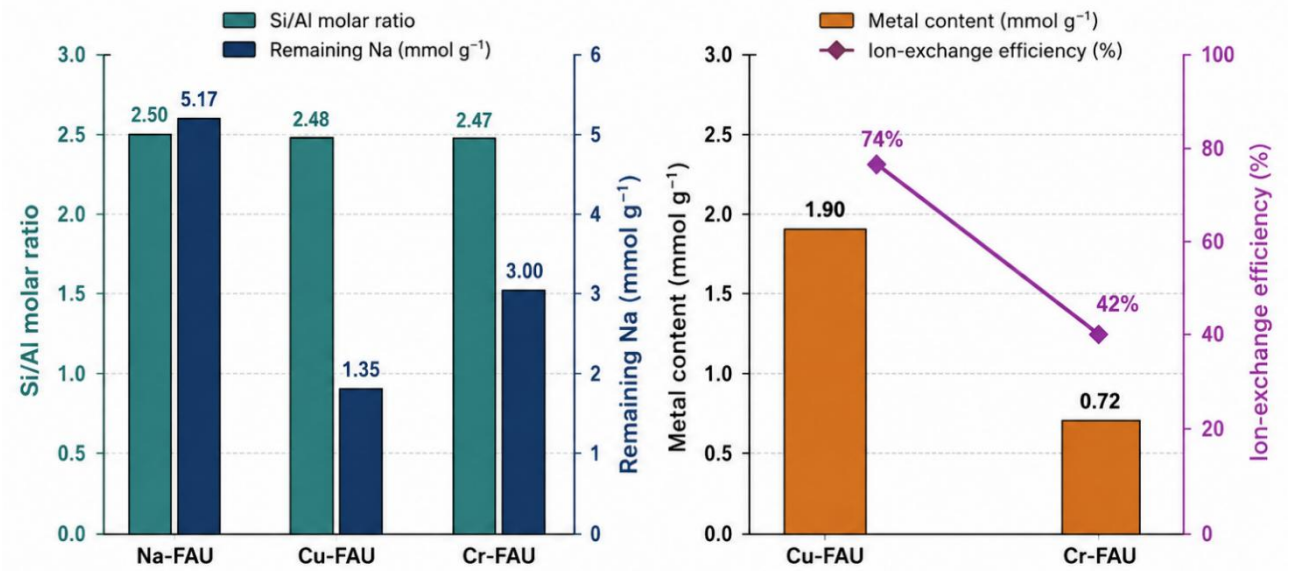


Figure 2. Chemical composition and ion-exchange characteristics of the Na-FAU, Cu-FAU and Cr-FAU samples: (a) oxide composition determined by XRF; (b) residual Na content, metal content calculated from the charge balance and degree of ion exchange.

The degree of ion exchange was calculated from the difference between the initial sodium content and the sodium content remaining after Exchange [34]:

$$IE(\%) = \frac{n_{\mathrm{Na,initial}} - n_{\mathrm{Na,residual}}}{n_{\mathrm{Na,initial}}} \times 100$$

where $n_{\mathrm{Na,initial}}$ is the Na content of the original Na-FAU sample and $n_{\mathrm{Na,residual}}$ is the Na content remaining in the metal-exchanged sample. Based on this approach, the degree of ion exchange for Cu-FAU was:

$$IE_{\mathrm{Cu-FAU}} = \frac{5.17 - 1.35}{5.17} \times 100 = 74\%$$

For Cr-FAU, it was:

$$IE_{\mathrm{Cr-FAU}} = \frac{5.17 - 3.00}{5.17} \times 100 = 42\%$$

Taking charge equivalence into account, the metal contents corresponding to the amount of replaced Na^+ were 1.91 mmol Cu g^{-1} for Cu-FAU and 0.72 mmol Cr g^{-1} for Cr-FAU:

$$n_{\mathrm{Cu}} = \frac{5.17 - 1.35}{2} = 1.91\ \mathrm{mmol\,g^{-1}}$$

$$n_{\mathrm{Cr}} = \frac{5.17 - 3.00}{3} = 0.72\ \mathrm{mmol\,g^{-1}}$$

These calculations assumed that each Cu^{2+} ion compensated for a framework charge equivalent to two Na^+ ions, while each Cr^{3+} ion compensated for a charge equivalent to three Na^+ ions.

Table 2. Chemical composition and ion-exchange parameters of the Na-FAU, Cu-FAU and Cr-FAU samples

Sample	**Si/Al molar ratio**	**Residual Na (mmol g^{-1})**	**Replaced Na^+ charge (mmol g^{-1})**	**Metal content based on charge balance (mmol g^{-1})**	**Degree of ion exchange (%)**
Na-FAU	2.50	5.17	—	—	—
Cu-FAU	2.48	1.35	3.82	1.91 Cu	74
Cr-FAU	2.47	3.00	2.17	0.72 Cr	42

The higher degree of ion exchange determined for Cu-FAU indicates that, under the applied exchange conditions, Cu^{2+} ions were incorporated into the accessible cation sites of Na-FAU more effectively than Cr^{3+} ions. The difference in the exchange behaviour of Cu^{2+} and Cr^{3+} cannot be explained solely by their ionic charges; hydration energy, hydrated ionic radius, hydrolysis equilibria in solution, precursor concentration and mass transfer within the zeolite must be considered together. In particular, the strong hydration and tendency towards hydrolysis of Cr^{3+} ions may restrict their transport to accessible exchange sites. However, confirming this mechanism would require a separate evaluation of the pH of the exchange solution and the state of the metal species in solution.

The combined analysis of the XRF, ICP-OES and PXRD results shows that metal modification was accompanied by a decrease in sodium content without any noticeable change in the Si/Al ratio or the principal FAU phase. Nevertheless, the chemical composition data do not determine the specific locations or degree of dispersion of the metal species within the zeolite. The spatial distributions of the Cu and Cr species should therefore be evaluated by SEM–EDS, while their local coordination and chemical states should be assessed together with the results of appropriate spectroscopic analyses.

4.3. Textural Properties — N_2 Physisorption and BET Analysis

The porous structures of the Na-FAU, Cu-FAU and Cr-FAU samples were evaluated by N_2 adsorption–desorption measurements at 77 K. Before analysis, the samples were degassed under vacuum at 300 °C for 6 hours to remove water and other volatile species adsorbed within the pores. The specific surface area was determined using the Brunauer–Emmett–Teller (BET) model, the total pore volume from the amount of nitrogen adsorbed at the specified relative pressure, and the micropore and external surface parameters using the t-plot method.

The N_2 adsorption–desorption isotherms of all three samples were characterised by a sharp increase in adsorption volume in the low-relative-pressure region. This behaviour indicates the rapid filling of micropores and corresponds to the Type I isotherm characteristic of FAU-type zeolites. The gradual increase in adsorption volume at medium and high relative pressures, together with the presence of a weakly defined hysteresis loop, may be attributed to the contribution of intercrystalline voids and a limited amount of textural mesoporosity [35].

The N_2 adsorption–desorption isotherms and pore-size distributions are presented in Figure 3. The higher adsorption capacity observed for Na-FAU at low relative pressure indicates that it had a larger accessible micropore volume than the ion-exchanged samples. Although the overall shape of the isotherms was retained after the incorporation of Cu^{2+} and Cr^{3+} ions, a decrease in the amount of adsorbed N_2 was observed. The largely unchanged isotherm shape indicates that ion exchange did not alter the overall pore characteristics of the FAU material, whereas the decrease in adsorption capacity

suggests a partial reduction in accessible micropore volume due to the location of transition-metal cations at pore entrances and intracrystalline cation sites.

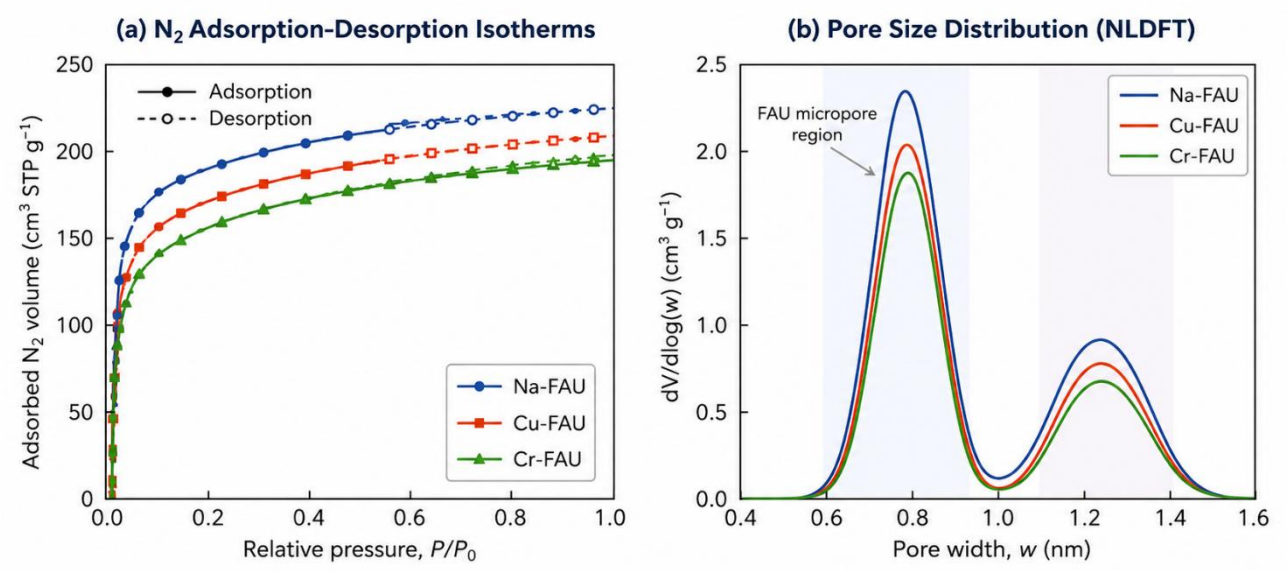


Figure 3. Textural properties of the Na-FAU, Cu-FAU and Cr-FAU samples: (a) N_2 adsorption–desorption isotherms at 77 K; (b) micropore-size distributions calculated using the NLDFT method.

According to the BET calculations, the specific surface area of Na-FAU was 721 $m^2\ g^{-1}$. The corresponding values for Cu-FAU and Cr-FAU were 654 and 628 $m^2\ g^{-1}$, respectively. Thus, compared with Na-FAU, the specific surface area decreased by approximately 9.3% for Cu-FAU and 12.9% for Cr-FAU. Nevertheless, the high surface areas retained by both ion-exchanged samples indicate that the porous structure of the FAU zeolite was largely preserved.

Table 3. Textural parameters of the Na-FAU, Cu-FAU and Cr-FAU samples determined by N_2 physisorption

Sample	S_{BET}($m^2\ g^{-1}$)	S_{micro}($m^2\ g^{-1}$)	S_{ext}($m^2\ g^{-1}$)	V_{micro}($cm^3\ g^{-1}$)	V_{total}($cm^3\ g^{-1}$)	V_{micro}/V_{total}(%)
Na-FAU	721	679	42	0.268	0.342	78.4
Cu-FAU	654	606	48	0.236	0.319	74.0
Cr-FAU	628	576	52	0.221	0.306	72.2

The micropore volume decreased from 0.268 $cm^3\ g^{-1}$ for Na-FAU to 0.236 $cm^3\ g^{-1}$ for Cu-FAU and 0.221 $cm^3\ g^{-1}$ for Cr-FAU. The total pore volume followed the same trend, with values of 0.342, 0.319 and 0.306 $cm^3\ g^{-1}$, respectively. The ratio of micropore volume to total pore volume was 78.4% for Na-FAU, 74.0% for Cu-FAU and 72.2% for Cr-FAU. These values indicate that micropores dominated the overall pore structure of all the materials, although their accessibility to adsorbate molecules decreased to some extent following metal exchange.

The increase in external surface area from 42 $m^2\ g^{-1}$ for Na-FAU to 48 $m^2\ g^{-1}$ for Cu-FAU and 52 $m^2\ g^{-1}$ for Cr-FAU is noteworthy. This change may be associated with local heterogeneities formed on the crystal surfaces, changes in the aggregation state of the particles during the ion-exchange and washing stages, and an increase in the relative contribution of intercrystalline voids. However, the

increase in external surface area cannot be regarded as direct evidence of the formation of a new ordered mesoporous system.

The NLDFT pore-size distributions show that the dominant micropore region associated with the FAU structure was retained in all three samples (Figure 3b). The absence of a noticeable shift in the position of the main pore-size distribution among the samples indicates that ion exchange did not reconstruct the geometrical pore system of the zeolite. Instead, the observed changes may mainly be explained by partial restriction of pore entrances and intracrystalline voids by metal cations and their coordination spheres.

The greater reductions in surface area and micropore volume observed for Cr-FAU suggest that Cr-containing species had a stronger effect on pore accessibility than Cu-containing species. However, because N_2 physisorption does not determine the specific crystallographic positions of metal cations, this conclusion should be regarded as a cautious interpretation based solely on the textural data. The location and distribution of the metal species should be evaluated together with the SEM–EDS and relevant spectroscopic results.

Overall, N_2 physisorption shows that although ion exchange with Cu^{2+} and Cr^{3+} caused moderate reductions in specific surface area and micropore volume, the high surface area and microporous character of Na-FAU were largely retained. These findings are consistent with the PXRD data and indicate that metal modification partially altered pore accessibility without disrupting the FAU framework. The preserved microporous structure provides the diffusion environment required for transporting ethanol molecules to the catalytic sites, while differences in surface area should be considered alongside the number and nature of the acid sites when interpreting catalytic behaviour [33].

4.4. Morphology and Elemental Distribution — SEM–EDS

The particle morphology of the Na-FAU, Cu-FAU and Cr-FAU samples was evaluated by scanning electron microscopy (SEM), while their surface elemental composition and elemental distribution were examined by energy-dispersive X-ray spectroscopy (EDS). Representative SEM micrographs and the corresponding EDS elemental maps of the samples are presented in Figure 4.

The SEM images of Na-FAU revealed well-defined polyhedral crystals, predominantly ranging from 1.2 to 2.5 μm in size. Most of the crystals exhibited the octahedral and truncated-octahedral morphologies characteristic of FAU-type zeolites. Although some aggregation was observed among individual particles, no noticeable morphological features indicating extensive cracking, severe erosion or the formation of an amorphous phase were detected on the crystal surfaces. These

observations are consistent with the PXRD results indicating the high crystallinity of the Na-FAU sample.

Following exchange with Cu^{2+} and Cr^{3+} ions, the overall crystal shape and size range were largely preserved. Crystal sizes were approximately 1.1–2.3 μm for Cu-FAU and 1.0–2.1 μm for Cr-FAU. The small differences in size observed among the samples should not be interpreted as an actual reduction in crystal size caused by ion exchange. Instead, they should be regarded as variations related to the statistical selection of the analysed particles, the aggregation state of the crystals and the limited field of view of the SEM images.

The retention of the octahedral morphology in the ion-exchanged samples indicates that the incorporation of Cu^{2+} and Cr^{3+} ions did not cause any noticeable morphological degradation of the zeolite crystals. No extensive collapse, severe surface corrosion or large aggregates attributable to separate metal oxide particles were observed in the Cu-FAU and Cr-FAU crystals. This finding supports the PXRD data presented in Section 4.1, which showed that the FAU crystalline phase was retained after ion exchange and that no crystalline CuO or Cr_2O_3 phases were detected [36].

The EDS elemental maps showed that the Si, Al and O signals were distributed consistently and relatively homogeneously throughout the analysed crystals. The similar spatial distributions of Si and Al indicate that the aluminosilicate framework was largely preserved after ion exchange and subsequent calcination. This result agrees with the Si/Al molar ratios determined by XRF, which were 2.50, 2.48 and 2.47 for Na-FAU, Cu-FAU and Cr-FAU, respectively.

In the Na-FAU sample, the broad distribution of the Na signal throughout the crystals was attributed to the presence of sodium cations compensating for the negative framework charge. Although the intensity of the Na signal decreased in the Cu-FAU and Cr-FAU samples, it did not disappear completely. This observation is consistent with the ICP-OES results: the Na content decreased from 5.17 mmol g^{-1} in the original Na-FAU sample to 1.35 mmol g^{-1} in Cu-FAU and 3.00 mmol g^{-1} in Cr-FAU. The presence of a residual Na signal confirms that ion exchange was partial rather than complete.

The Cu signal in the Cu-FAU sample and the Cr signal in the Cr-FAU sample were broadly and relatively uniformly distributed across the surfaces of the selected crystals. Although local variations in intensity were observed in the metal maps, no sharply localised regions indicating the formation of separate micrometre-sized Cu- or Cr-rich aggregates were detected. This result indicates that the transition metals were dispersed throughout the crystals, at least within the spatial resolution of SEM–EDS analysis. However, EDS mapping cannot distinguish whether the metal cations are located on the external surfaces, within the micropores or at specific crystallographic exchange sites in the zeolite crystals.

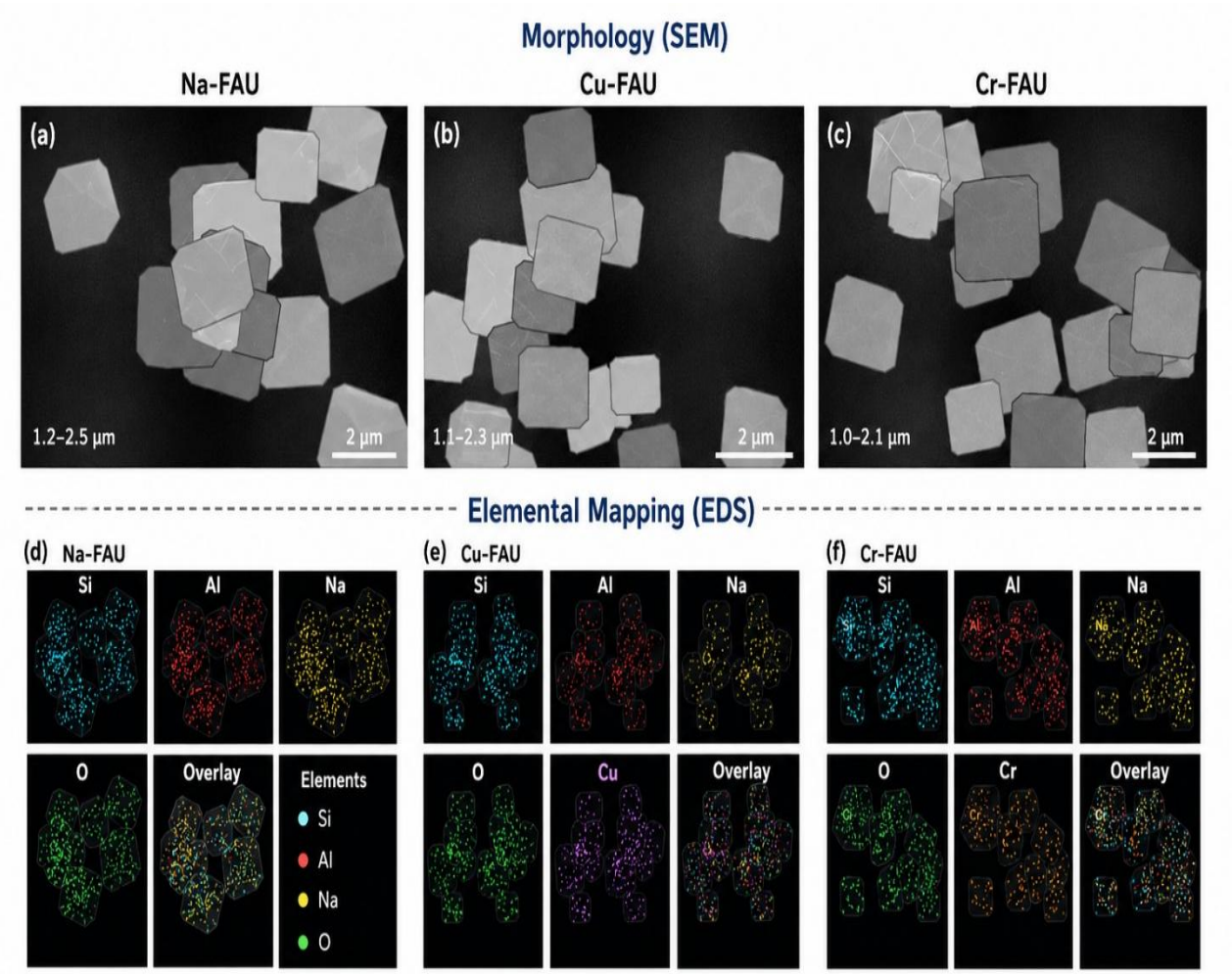


Figure 4. Morphological and elemental characterisation of the Na-FAU, Cu-FAU and Cr-FAU samples: (a–c) SEM micrographs of the corresponding samples; (d–f) EDS maps of Si, Al, Na and O, together with Cu for Cu-FAU and Cr for Cr-FAU.

Scale bars are shown in the corresponding micrographs.

Table 4. Morphological and elemental characteristics of the Na-FAU, Cu-FAU and Cr-FAU samples determined by SEM–EDS

Sample	**Approximate crystal size (µm)**	**Principal morphology**	**Residual Na signal**	**Metal distribution determined by EDS**	**Large metal-rich aggregates**
Na-FAU	1.2–2.5	Octahedral and truncated-octahedral crystals	Strong	Not applicable	Not detected
Cu-FAU	1.1–2.3	Largely retained octahedral morphology	Weaker but still present	Cu signal broadly and relatively homogeneously distributed throughout the crystals	Not detected

Cr-FAU	1.0–2.1	Largely retained octahedral morphology	More pronounced than in Cu-FAU	Cr signal broadly and relatively homogeneously distributed throughout the crystals	Not detected

The weaker Na signal in Cu-FAU than in Cr-FAU is consistent with their respective ion-exchange degrees of 74% and 42%. In other words, the higher exchange efficiency of Cu^{2+} ions resulted in a lower residual Na signal in the Cu-FAU sample. The more pronounced residual Na signal observed in Cr-FAU can be explained by the lower degree of ion exchange in this sample.

The combined evaluation of the SEM results and N_2 physisorption data shows that although the external morphology of the crystals was retained after ion exchange, the accessible micropore volume decreased to some extent. The micropore volume decreased from 0.268 $cm^3\ g^{-1}$ for Na-FAU to 0.236 $cm^3\ g^{-1}$ for Cu-FAU and 0.221 $cm^3\ g^{-1}$ for Cr-FAU. The absence of severe morphological degradation in the SEM images suggests that this reduction did not result from crystal collapse but from the partial restriction of pore accessibility caused by the location of the exchanged cations at pore entrances and intracrystalline sites. The increase in external surface area from 42 $m^2\ g^{-1}$ for Na-FAU to 48 $m^2\ g^{-1}$ for Cu-FAU and 52 $m^2\ g^{-1}$ for Cr-FAU may be associated with changes in the aggregation state of the particles and the relative contribution of intercrystalline voids.

Overall, the SEM–EDS results show that exchange with Cu^{2+} and Cr^{3+} ions occurred without disrupting the principal morphology of the FAU crystals and that the metal species were broadly distributed throughout the analysed crystals. When considered together with the PXRD, XRF/ICP-OES and N_2 physisorption data, these results confirm that metal modification altered mainly the extra-framework cation composition and pore accessibility without disrupting the aluminosilicate framework. However, determining the atomic-level coordination environments and specific crystallographic positions of the metal cations requires the EDS results to be complemented by XPS, X-ray absorption spectroscopy or other local structural analyses.

4.5. Framework Structure and Local Coordination — FTIR and MAS NMR

The aluminosilicate framework structures of the Na-FAU, Cu-FAU and Cr-FAU samples were evaluated by FTIR spectroscopy, while the local coordination environments of the Al and Si atoms were examined by solid-state ^{27}Al and ^{29}Si MAS NMR spectroscopy. These methods allow the effects of ion exchange and subsequent thermal treatment on the integrity of the FAU framework, the coordination state of framework aluminium and the local chemical environment of silicon to be determined. The corresponding FTIR and MAS NMR spectra are presented in Figure 5.

The principal vibrational bands associated with the FAU-type aluminosilicate framework were observed in the FTIR spectra of all three samples. The intense absorption band recorded at approximately 1000–1100 cm^{-1} was assigned to the asymmetric T–O–T stretching vibrations of Si–O–Si and Si–O–Al bonds within the framework, where T represents a tetrahedrally coordinated Si or Al atom. The bands at approximately 720–790 cm^{-1} correspond to symmetric T–O–T stretching, while the signals in the region of 450–470 cm^{-1} are associated with the bending vibrations of T–O bonds. The retention of the band at approximately 565–580 cm^{-1}, which is associated with the double six-membered-ring structural units of the FAU topology, in all samples indicates that the zeolite framework was largely preserved after ion exchange.

The similar spectral profiles exhibited by the Na-FAU, Cu-FAU and Cr-FAU samples in the framework vibration region indicate that the incorporation of Cu^{2+} and Cr^{3+} ions did not cause extensive structural changes in the aluminosilicate network. The slight differences observed in the positions, intensities and widths of some bands in the metal-exchanged samples may be attributed not to framework reconstruction but to changes in the local T–O–T environments resulting from electrostatic interactions between the extra-framework cations and framework oxygen atoms.

The broad absorption band observed at approximately 3400–3500 cm^{-1} is associated with the O–H stretching vibrations of surface hydroxyl groups and water molecules adsorbed within the pores. The band in the region of approximately 1630–1650 cm^{-1} is attributed to the H–O–H bending vibration of adsorbed water. Differences in the intensities and widths of these bands indicate changes in the degree of hydration of the samples and in the interactions between extra-framework cations and water molecules. The relatively broad OH region of Cr-FAU may be explained by the strong hydration of Cr^{3+} ions and the formation of more heterogeneous local hydroxyl environments. However, because the absorption bands of water and different hydroxyl groups overlap in this region, Brønsted and Lewis acid sites cannot be quantified separately using conventional FTIR spectra.

A dominant resonance at approximately 58–62 ppm was observed in the solid-state ^{27}Al MAS NMR spectra of all three samples. This signal is assigned to tetrahedrally coordinated Al(IV) species incorporated into the FAU framework. The retention of the tetrahedral Al resonance after ion exchange indicates that most of the aluminium atoms remained within the framework and that the exchange–calcination procedures did not cause extensive dealumination.

The absence of a noticeable resonance near 0 ppm corresponding to octahedrally coordinated extra-framework Al(VI) species in the Na-FAU and Cu-FAU samples indicates that no substantial framework disruption occurred in these materials. The very weak additional signal observed near 0 ppm in the Cr-FAU spectrum suggests that trace amounts of extra-framework Al(VI) species may have formed. However, the very low intensity of this signal relative to the principal Al(IV) resonance does not provide sufficient evidence that the FAU framework underwent significant dealumination.

The paramagnetic properties of Cu^{2+} and Cr^{3+} ions should also be considered when interpreting the ^{27}Al MAS NMR spectra of the metal-exchanged samples. The relaxation times of Al nuclei located near these ions may be shortened, their resonances may broaden and their signal intensities may decrease. Therefore, possible broadening and intensity changes in the Cu-FAU and Cr-FAU spectra should not be interpreted directly as a decrease in the framework Al content. These changes may also arise from the paramagnetic effects of the extra-framework metal cations.

The ^{29}Si MAS NMR spectra consist of overlapping resonances from $Q^4(nAl)$ silicon environments associated with different numbers of Al atoms within the FAU framework. Contributions at approximately −89, −94, −99, −104 and −109 ppm may be assigned to Si(4Al), Si(3Al), Si(2Al), Si(1Al) and Si(0Al) environments, respectively. In FAU materials with a Si/Al molar ratio of approximately 2.5, Q^4 species associated with Al atoms are expected to make a noticeable contribution to the spectrum.

The similarity of the principal resonance positions and overall spectral envelopes in the ^{29}Si MAS NMR spectra of Na-FAU, Cu-FAU and Cr-FAU indicates that the local coordination environment of the silicon atoms did not change substantially after ion exchange. This result agrees with the Si/Al molar ratios determined by XRF, which were 2.50, 2.48 and 2.47 for Na-FAU, Cu-FAU and Cr-FAU, respectively. The absence of new and intense Q^3 resonances in the metal-exchanged samples indicates that large numbers of Si–OH-type framework defects were not formed and that the silicon–oxygen network did not undergo extensive hydrolytic degradation.

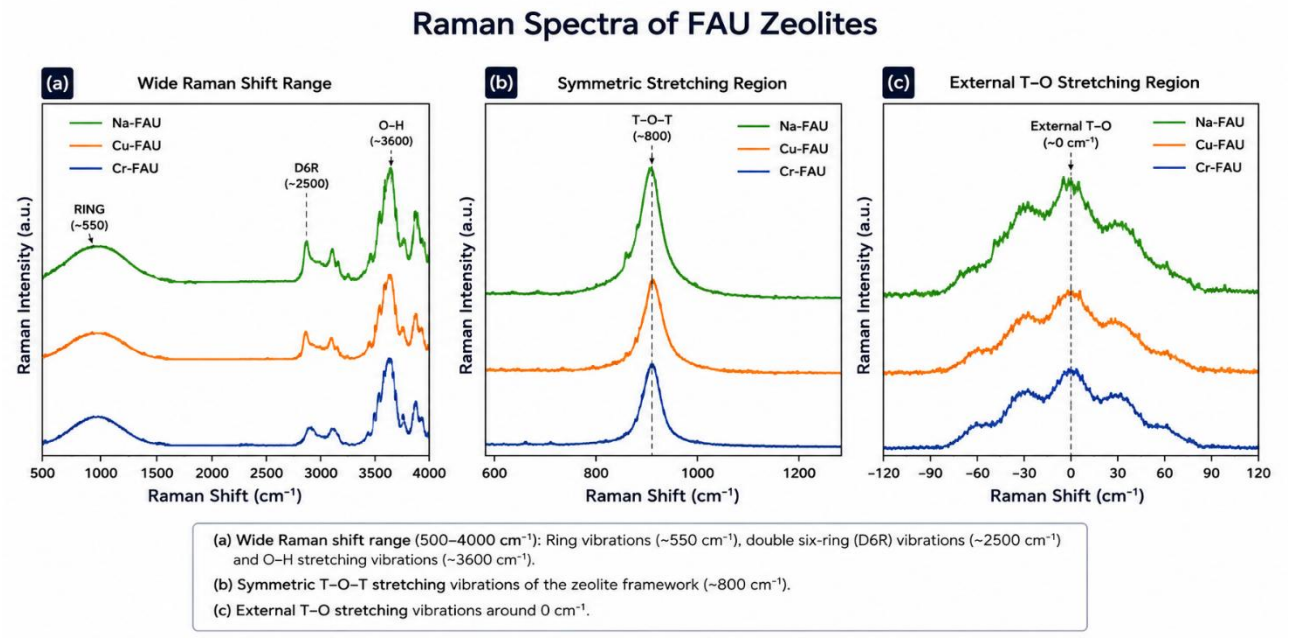


Figure 5. Framework structure and local coordination environments of the Na-FAU, Cu-FAU and Cr-FAU samples: (a) FTIR spectra showing the principal vibrational bands of the aluminosilicate framework; (b) ^{27}Al MAS NMR spectra showing tetrahedral framework Al(IV) and possible extra-framework Al(VI) species; (c) ^{29}Si MAS NMR spectra showing the $Q^4(nAl)$ silicon environments within the FAU framework.

Table 5. Principal structural features identified by FTIR and MAS NMR analyses

Analysis	Spectral region	Assignment	Structural interpretation
FTIR	3400–3500 cm^{-1}	O–H stretching vibrations and adsorbed water	Degree of hydration and hydroxyl environments
FTIR	1630–1650 cm^{-1}	H–O–H bending vibration	Water adsorbed within the pores
FTIR	1000–1100 cm^{-1}	Asymmetric T–O–T stretching vibration	Principal vibrational region of the aluminosilicate framework
FTIR	720–790 cm^{-1}	Symmetric T–O–T stretching vibration	Retention of framework bonds
FTIR	565–580 cm^{-1}	Double six-membered-ring vibration	Retention of the FAU topology
FTIR	450–470 cm^{-1}	T–O bending vibration	Low-frequency vibration of the zeolite framework
^{27}Al MAS NMR	58–62 ppm	Tetrahedral Al(IV)	Dominant coordination state of framework aluminium
^{27}Al MAS NMR	Approximately 0 ppm	Octahedral Al(VI)	Extra-framework Al; possible trace contribution in Cr-FAU
^{29}Si MAS NMR	−89 to −109 ppm	Q^4(nAl) silicon environments	Framework Si species with different Al environments

The combined evaluation of the FTIR and MAS NMR results with the PXRD, XRF/ICP-OES, SEM–EDS and N_2 physisorption data indicates that exchange with Cu^{2+} and Cr^{3+} ions did not disrupt the principal aluminosilicate framework of the FAU zeolite. The observed spectral differences are attributed to the hydration of extra-framework cations, their interactions with framework oxygen atoms and the resulting changes in the local coordination environment rather than to extensive structural transformations. Despite the possible trace Al(VI) signal in Cr-FAU, the predominance of tetrahedral Al(IV) and Q^4(nAl) environments confirms that the FAU framework was largely retained in both metal-exchanged samples.

4.6. Nature and Concentration of Acid Sites — Py-FTIR and NH_3-TPD

The acidic properties of the Na-FAU, Cu-FAU and Cr-FAU samples were evaluated by pyridine-adsorbed FTIR spectroscopy (Py-FTIR) and ammonia temperature-programmed desorption (NH_3-TPD). Py-FTIR was used to distinguish the nature and relative proportions of Brønsted and Lewis acid sites, while NH_3-TPD was used to determine the total concentration and strength distribution of the acid sites. The combined application of these two methods allows the effect of ion exchange on both the acid-site composition of the FAU zeolites and the strength of their interaction with ammonia to be evaluated comparatively. The corresponding Py-FTIR spectra and NH_3-TPD profiles are presented in Figure 6.

The FTIR spectra recorded after pyridine adsorption and evacuation at 350 °C showed characteristic absorption bands at approximately 1450 and 1545 cm^{-1}. The band at approximately 1450 cm^{-1} was assigned to pyridine coordinated to coordinatively unsaturated metal or extra-framework cation sites and, therefore, to Lewis acid sites. The band observed at approximately 1545 cm^{-1} corresponds to pyridine protonated at Brønsted acid sites to form pyridinium ions. The band in the region of approximately 1490 cm^{-1} reflects the combined contributions of pyridine coordinated to Lewis acid sites and pyridinium species formed at Brønsted acid sites.

Signals corresponding to both Lewis and Brønsted acid sites were observed in the Na-FAU sample. Lewis acidity in Na-FAU may mainly be associated with the interaction of extra-framework Na^{+} cations and possible coordinatively unsaturated Al species with pyridine. Brønsted acidity is associated with residual protonic hydroxyl groups, surface silanol groups and proton-donating sites formed through the dissociative interaction of water. However, as Na-FAU is not the protonic form of FAU, its Brønsted acidity is expected to be limited.

Following exchange with Cu^{2+} ions, the relative intensity of the Lewis band at 1450 cm^{-1} increased substantially. When the integrated area of this band for Na-FAU was taken as 1.00, the normalised relative intensity for Cu-FAU was 1.72. This increase is attributed to the formation of coordinatively unsaturated Cu-containing sites capable of accepting the lone electron pair on the nitrogen atom of the pyridine molecule. At the same time, the relative intensity of the Brønsted band at 1545 cm^{-1} in Cu-FAU decreased to 0.61 relative to Na-FAU. This change may be explained by a reduction in the relative proportion of proton-donating hydroxyl environments during ion exchange and the predominance of Lewis-acidic Cu sites.

In the Cr-FAU sample, the normalised relative intensity of the band corresponding to Lewis acid sites was 1.55. This value indicates an increase in Lewis acidity relative to Na-FAU, although the increase was slightly lower than that observed for Cu-FAU. The relative intensity of the Brønsted band in Cr-FAU was 0.79, indicating that a greater Brønsted contribution was retained than in Cu-FAU. This feature may be associated with the lower degree of Cr^{3+} exchange, the strong hydration of Cr-containing species and the presence of a greater amount of residual Na^{+} and hydroxyl environments in the sample. However, because the Py-FTIR results do not determine the specific coordination structure of the Cr species, this explanation should be regarded as a cautious interpretation.

Table 6. Normalised relative intensities of Brønsted and Lewis acid sites determined by Py-FTIR

Sample	**Lewis band at approximately 1450 cm^{-1}**	**Brønsted band at approximately 1545 cm^{-1}**	**Relative L/B ratio**
Na-FAU	1.00	1.00	1.00
Cu-FAU	1.72	0.61	2.82
Cr-FAU	1.55	0.79	1.96

The values presented in the table are relative values obtained by normalising the integrated band areas measured under identical initial sample mass, spectral acquisition and evacuation conditions to those of Na-FAU. Therefore, they represent comparative changes among the samples rather than the absolute concentrations of acid sites. Calculating the absolute concentration of acid sites by Py-FTIR requires consideration of the sample mass, disc area and thickness, as well as the corresponding molar absorption coefficients of pyridine adsorbed at Brønsted and Lewis acid sites.

Comparison of the Py-FTIR results shows that the relative distribution of the acid sites changed in the following order:

Lewis acidity: Cu-FAU > Cr-FAU > Na-FAU

Brønsted acidity: Na-FAU > Cr-FAU > Cu-FAU

The high relative L/B ratio calculated for Cu-FAU indicates the predominance of Lewis-acidic sites in this sample, whereas the intermediate value obtained for Cr-FAU indicates a more balanced distribution of Lewis and Brønsted sites. However, because the L/B ratio is based only on normalised band areas, it should not be presented as an absolute acid-site ratio without accounting for the different molar absorption coefficients of the pyridine complexes [37].

The total concentration and strength distribution of the acid sites were determined by NH_3-TPD. Two principal signals located in the low- and high-temperature regions were observed in the desorption profiles of all three samples. The low-temperature desorption maxima were recorded in the range of 238–245 °C, while the high-temperature maxima occurred between 422 and 447 °C.

The low-temperature desorption region is associated with the removal of ammonia adsorbed at weak and medium-strength acid sites. This region may include contributions from surface hydroxyl groups, weak Lewis-acidic extra-framework cations and physically adsorbed species. The high-temperature desorption region is assigned to acid sites that retain ammonia more strongly, including stronger Lewis acid sites and proton-donating hydroxyl environments. As NH_3 interacts with both Brønsted and Lewis acid sites, NH_3-TPD profiles do not distinguish between these sites separately.

For Na-FAU, the low- and high-temperature desorption maxima were observed at 238 and 422 °C, respectively. The total acidity was 0.58 mmol NH_3 g^{-1}, while the ratio between the integrated areas of the low- and high-temperature peaks (LT/HT) was 1.40. This result indicates the relative predominance of weak and medium-strength acid sites in Na-FAU.

For Cu-FAU, the low-temperature maximum shifted to 245 °C and the high-temperature maximum to 447 °C. The total acidity increased to 0.84 mmol NH_3 g^{-1}, representing an increase of approximately 45% relative to Na-FAU. At the same time, the LT/HT ratio decreased to 0.80. The increased relative contribution of the high-temperature region and the shift of the desorption maximum towards a higher temperature indicate that the proportion of sites interacting more strongly

with ammonia increased following Cu^{2+} exchange. This result agrees with the Py-FTIR data showing increased Lewis acidity in Cu-FAU.

For Cr-FAU, the low- and high-temperature maxima were identified at 242 and 438 °C, respectively. The total acidity of this sample was 0.91 mmol NH_3 g^{-1}, the highest value among the samples examined. The increase in total acidity relative to Na-FAU was approximately 57%. The LT/HT ratio of 1.10 indicates that both low- and high-temperature acid sites made substantial contributions in Cr-FAU. This result is consistent with the more balanced Lewis–Brønsted distribution identified by Py-FTIR analysis.

Table 7. Acidity parameters obtained from NH_3-TPD analysis

Parameter	**Na-FAU**	**Cu-FAU**	**Cr-FAU**
LT maximum temperature (°C)	238	245	242
HT maximum temperature (°C)	422	447	438
Total acidity (mmol NH_3 g^{-1})	0.58	0.84	0.91
Increase relative to Na-FAU (%)	—	45	57
LT/HT peak-area ratio	1.40	0.80	1.10

According to the NH_3-TPD results, total acidity followed the order:

$$\text{Cr-FAU} > \text{Cu-FAU} > \text{Na-FAU}$$

However, the highest total acidity does not necessarily correspond to the highest catalytic activity. Although NH_3-TPD indicates the total concentration of acid sites and their apparent strength distribution based on the ammonia desorption temperature, it does not separately identify their Brønsted or Lewis character. Furthermore, because the NH_3 molecule has a small kinetic diameter, it may access certain internal sites that are inaccessible to larger ethanol and pyridine molecules. Therefore, the interpretation of catalytic behaviour should consider not only the total number of acid sites but also their nature, strength, location within the pores and accessibility to the reactant molecules.

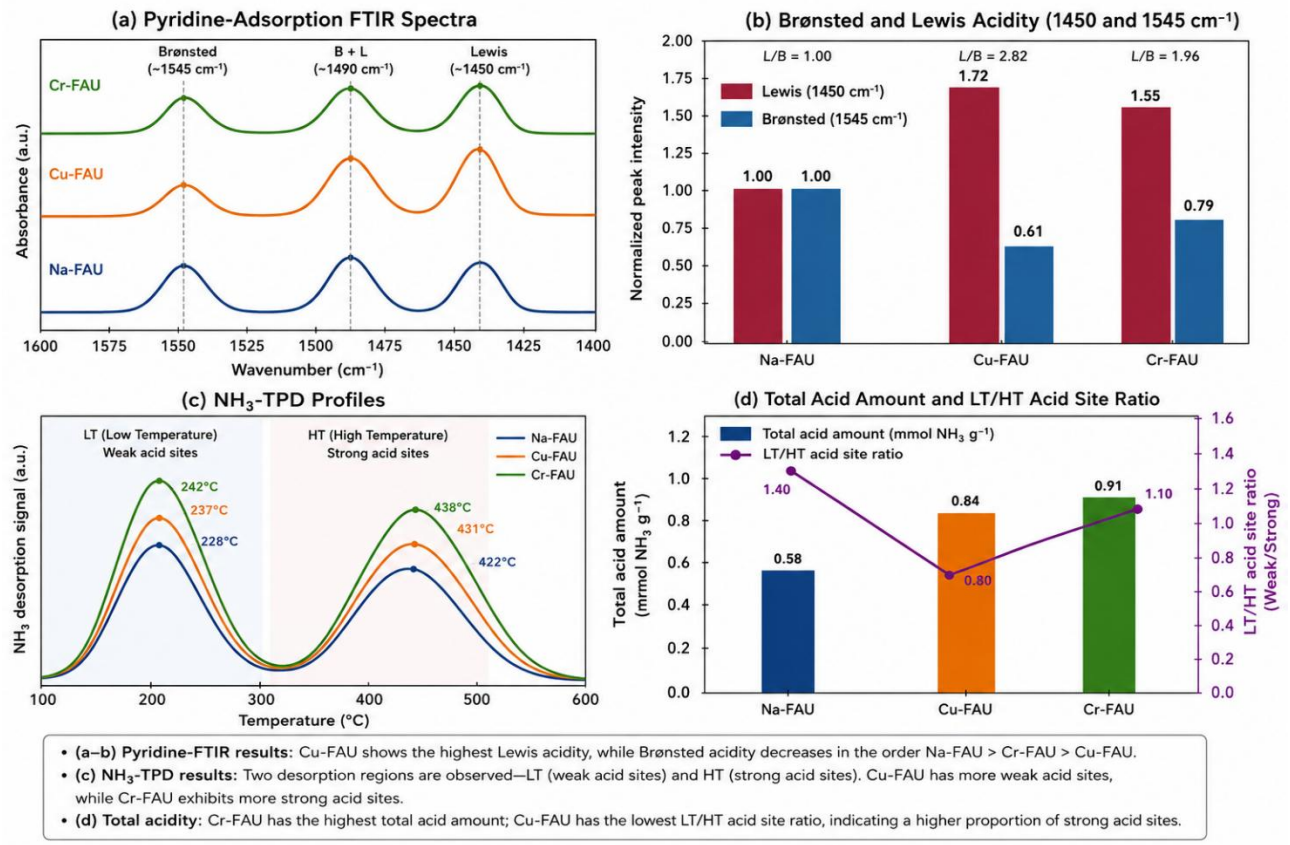


Figure 6. Acidic properties of the Na-FAU, Cu-FAU and Cr-FAU samples: (a) Py-FTIR spectra recorded after evacuation at 350 °C; (b) normalised relative intensities of Lewis and Brønsted acid sites determined from the bands at approximately 1450 and 1545 cm⁻¹; (c) NH₃-TPD profiles; (d) comparison of total acidity and the LT/HT peak-area ratio.

Overall, the Py-FTIR and NH₃-TPD results show that exchange with Cu^{2+} and Cr^{3+} ions substantially altered the acidic properties of the FAU zeolites. Cu-FAU exhibited a greater increase in the relative proportion of Lewis acid sites and in the high-temperature NH_3 desorption contribution. Cr-FAU showed the highest total NH_3 uptake together with a broader distribution of weak and strong acid sites. Thus, ion exchange not only increased the number of acid sites but also altered their nature and strength distribution according to the properties of the exchanged metal cation.

4.7. Thermal Behaviour — TGA/DTG

The thermal behaviour of the Na-FAU, Cu-FAU and Cr-FAU samples was evaluated by thermogravimetric analysis (TGA) and derivative thermogravimetric analysis (DTG) over the temperature range of 30–800 °C. The TGA curves show changes in sample mass with increasing temperature, while the DTG profiles identify the temperature regions in which the individual mass-loss stages occurred at their maximum rates. The corresponding TGA and DTG curves are presented in Figure 7, while the mass-loss values calculated for each stage are provided in Table 8.

Three main, partially overlapping mass-loss stages were observed in the TGA profiles of all samples. The continuous and gradual nature of the mass loss indicates that no abrupt thermal decomposition

occurred. The retention of the principal inorganic aluminosilicate mass as the temperature increased to 800 °C indicates the thermal stability of the Na-FAU, Cu-FAU and Cr-FAU samples over a wide temperature range.

The first mass-loss stage extended from room temperature to approximately 180 °C. This stage is mainly associated with the removal of water physically adsorbed on the external surfaces of the crystals and within the micropores of the zeolite. The large supercages, hydrophilic aluminosilicate framework and extra-framework charge-compensating cations of FAU zeolite provide a favourable environment for water adsorption. Therefore, low-temperature mass loss depends substantially on the initial hydration state of the samples.

During this stage, the Na-FAU sample exhibited a mass loss of approximately 6.5%. The corresponding values for Cu-FAU and Cr-FAU were approximately 4.0% and 5.3%, respectively. The higher low-temperature mass loss of Na-FAU may be associated with its larger accessible micropore volume. According to the N_2 physisorption results, the micropore volume of Na-FAU was 0.268 $cm^3\ g^{-1}$, compared with 0.236 $cm^3\ g^{-1}$ for Cu-FAU and 0.221 $cm^3\ g^{-1}$ for Cr-FAU. The location of metal cations at pore entrances and intracrystalline sites may partially reduce the pore volume accessible to water.

However, because low-temperature mass loss does not depend solely on pore volume, the differences among the samples should not be regarded as an absolute measure of their water adsorption capacity. Sample storage conditions, the duration of exposure to the atmosphere before analysis, the hydration energy of the cations and the applied predrying procedure may also affect this value. The greater mass loss of Cr-FAU compared with Cu-FAU may be associated with the stronger hydration of Cr^{3+}-containing species and their retention of a greater amount of water within their coordination spheres [38, 39].

The second mass-loss stage was observed over the temperature range of approximately 180–500 °C. The gradual decrease in mass in this region may be associated with the removal of coordinated water molecules interacting more strongly with extra-framework Na^+, Cu^{2+} and Cr^{3+} cations, as well as the condensation of weakly bound surface hydroxyl species. During this stage, the mass losses of Na-FAU, Cu-FAU and Cr-FAU were approximately 3.0%, 2.9% and 2.7%, respectively. The small differences among the samples indicate that the overall contributions of the processes occurring within this temperature range were similar.

The third stage covered the temperature range of 500–800 °C. The mass loss observed in this region may be associated with the condensation of more strongly bound hydroxyl groups, the dehydroxylation of metal–hydroxyl species and the removal of residual water species. Mass losses of approximately 4.0%, 4.0% and 4.1% were recorded for Na-FAU, Cu-FAU and Cr-FAU, respectively.

The similarity of the high-temperature mass losses indicates that the principal aluminosilicate structures of all samples exhibited similar thermal behaviour.

Weak high-temperature maxima were observed in the DTG profiles of Cu-FAU and Cr-FAU at approximately 628 and 641 °C, respectively. These maxima may be associated with the condensation of hydroxyl species linked to the metal cations or the removal of strongly bound residual water species. The location of the Cr-FAU maximum at a higher temperature is consistent with the relatively stronger retention of water and hydroxyl species in local Cr-containing environments. However, these maxima cannot be assigned unambiguously on the basis of TGA/DTG results alone, and coupled gas analysis by mass spectrometry or FTIR would be required.

Table 8. Mass-loss values for the individual stages determined from the TGA curves of the Na-FAU, Cu-FAU and Cr-FAU samples

Sample	**Stage I: 30–180 °C (%)**	**Stage II: 180–500 °C (%)**	**Stage III: 500–800 °C (%)**	**Total mass loss (%)**	**Residual mass at 800 °C (%)**
Na-FAU	≈6.5	≈3.0	≈4.0	≈13.6	≈86.3
Cu-FAU	≈4.0	≈2.9	≈4.0	≈10.9	≈89.1
Cr-FAU	≈5.3	≈2.7	≈4.1	≈12.0	≈88.0

As the stage-specific and total values presented in the table were estimated from the TGA curves, rounding may result in differences of approximately 0.1 percentage points between their sums.

The total mass loss of the Na-FAU sample was approximately 13.6%, and approximately 86.3% of its initial mass was retained at 800 °C. For Cu-FAU, the total mass loss was 10.9%, while the residual mass was 89.1%. The corresponding values for Cr-FAU were approximately 12.0% and 88.0%. Thus, the total mass loss followed the order:

$$\text{Na-FAU} > \text{Cr-FAU} > \text{Cu-FAU}$$

The higher residual masses of the metal-exchanged samples at 800 °C may be associated with their lower initial water contents, reduced micropore accessibility and the presence of non-volatile metal species. Therefore, it would not be appropriate to conclude solely from the higher residual mass that Cu-FAU and Cr-FAU possessed greater structural thermal stability than Na-FAU. Confirming structural stability would require PXRD, FTIR or MAS NMR analyses after thermal treatment.

The absence of sharp and substantial mass-loss events in the TGA curves indicates that the samples did not contain significant amounts of residual organic matter or thermally unstable precursor species. This finding suggests that the washing and calcination stages following ion exchange were effective in removing the metal nitrate precursors and weakly bound species. However, TGA analysis alone

does not confirm the complete chemical absence of residual nitrates; appropriate spectroscopic or gas-analysis results would be required for this purpose.

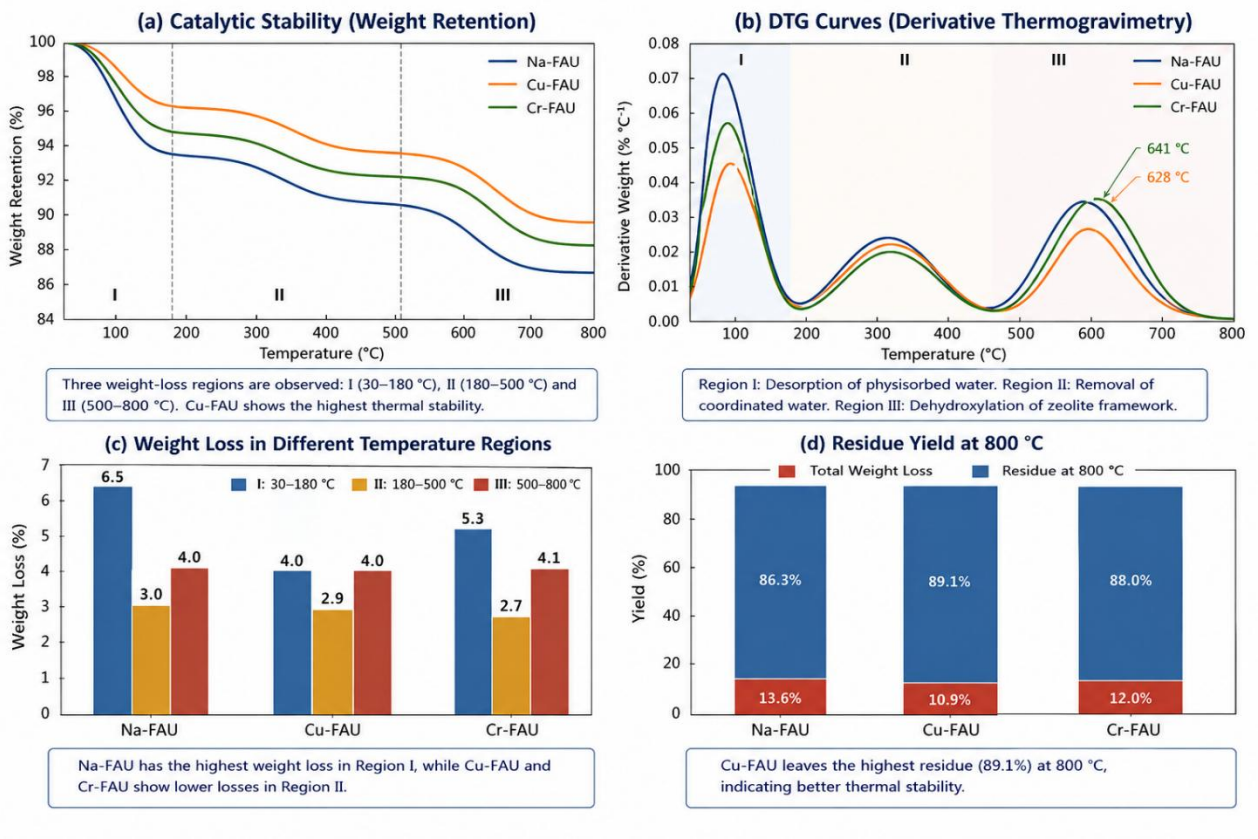


Figure 7. Thermal behaviour of the Na-FAU, Cu-FAU and Cr-FAU samples: (a) TGA curves recorded over the temperature range of 30–800 °C; (b) DTG profiles showing the principal mass-loss stages and characteristic maxima; (c) comparison of mass losses at each stage; (d) total mass loss and residual mass at 800 °C.

Overall, the TGA/DTG results show that the Na-FAU, Cu-FAU and Cr-FAU samples largely retained their principal inorganic mass up to 800 °C. The main difference among the samples was observed during the low-temperature water-loss stage, with the metal-exchanged samples exhibiting lower total mass losses than Na-FAU. The absence of additional abrupt decomposition stages in the high-temperature region indicates that ion exchange did not generate substantial amounts of thermally unstable species in the FAU materials. When considered together with the PXRD, FTIR, MAS NMR and N_2 physisorption data, these results support the conclusion that the FAU-based porous structure was largely preserved under the thermal treatment conditions following metal modification.

4.8. Ethanol Conversion and Product Selectivity

The catalytic behaviour of the Na-FAU, Cu-FAU and Cr-FAU samples was evaluated in the gas-phase conversion of ethanol over the temperature range of 200–450 °C. The experiments were conducted in a fixed-bed reactor using N_2 as the carrier gas at a weight hourly space velocity of 2.0

$g_{EtOH}\ g_{catalyst}^{-1}\ h^{-1}$. The catalytic results were compared in terms of ethanol conversion, carbon-based selectivity towards the principal products and the corresponding product yields.

Ethanol conversion was calculated using the following expression:

$$X_{\mathrm{EtOH}}(\%) = \frac{F_{\mathrm{EtOH,in}} - F_{\mathrm{EtOH,out}}}{F_{\mathrm{EtOH,in}}} \times 100$$

where $F_{\mathrm{EtOH,in}}$and $F_{\mathrm{EtOH,out}}$are the molar flow rates of ethanol entering and leaving the reactor, respectively.

Product selectivity was determined on the basis of the carbon balance as follows:

$$S_i(\%) = \frac{n_{C,i}F_i}{\sum_j n_{C,j}\,F_j} \times 100$$

where $F_i$is the molar flow rate of the corresponding product and $n_{C,i}$is the number of carbon atoms in the product molecule. Product yield was calculated from the product of ethanol conversion and the selectivity towards the corresponding product:

$$Y_i(\%) = \frac{X_{\mathrm{EtOH}}S_i}{100}$$

Effect of Temperature on Ethanol Conversion

Ethanol conversion increased with increasing temperature over all the catalysts. Across the investigated temperature range, catalytic activity generally followed the order:

Cu-FAU > Cr-FAU > Na-FAU

Na-FAU exhibited the lowest catalytic activity, with an ethanol conversion of 62% at 350 °C. The incorporation of Cu^{2+} and Cr^{3+} ions resulted in a substantial increase in conversion. At the same temperature, conversions of 91% and 79% were recorded for Cu-FAU and Cr-FAU, respectively. Thus, relative to Na-FAU, conversion at 350 °C increased by 29 percentage points for Cu-FAU and 17 percentage points for Cr-FAU.

When the temperature was increased to 450 °C, conversion reached 98% for Cu-FAU and 94% for Cr-FAU. The almost complete conversion achieved over Cu-FAU indicates that acid sites favourable for the activation of ethanol molecules were formed in this sample. Although Cr-FAU also provided high conversion, its activity remained lower than that of Cu-FAU under all comparative conditions.

Table 9. Ethanol conversion over the Na-FAU, Cu-FAU and Cr-FAU catalysts

Sample	Conversion at 350 °C (%)	Conversion at 450 °C (%)	Overall activity ranking
Na-FAU	62	—	3
Cu-FAU	91	98	1
Cr-FAU	79	94	2

The precise ethanol conversion value for Na-FAU at 450 °C was not provided and is therefore not included in the table. The high activity of Cu-FAU cannot be explained solely by its total surface area. Although the BET surface area was 721 $m^2\ g^{-1}$ for Na-FAU, it decreased to 654 $m^2\ g^{-1}$ for Cu-FAU. Despite this reduction, Cu-FAU exhibited higher conversion. This result indicates that catalytic activity was governed more strongly by the chemical nature and strength of the active sites than by the absolute surface area.

In the Py-FTIR analysis, the normalised intensity of the band corresponding to Lewis acid sites increased to 1.72 for Cu-FAU, while the relative Lewis/Brønsted ratio was 2.82. The NH_3-TPD results also showed that the total acidity of Cu-FAU reached 0.84 mmol $NH_3\ g^{-1}$ and that the relative contribution of the high-temperature desorption region increased. These characteristics indicate that coordinatively unsaturated Cu-containing Lewis sites facilitated the interaction with the hydroxyl oxygen of ethanol and the subsequent conversion of the molecule.

Although Cr-FAU had the highest total acidity, at 0.91 mmol $NH_3\ g^{-1}$, its ethanol conversion was lower than that of Cu-FAU. This observation confirms that the total acidity determined by NH_3-TPD alone does not explain catalytic activity. The Lewis or Brønsted nature of the acid sites, their strength distribution, the redox properties of the metal cations and their accessibility to ethanol molecules must be considered together.

Product Selectivity

During ethanol conversion, dehydration and dehydrogenation were the principal reactions. Ethylene was formed through the intramolecular dehydration of ethanol, diethyl ether through intermolecular dehydration and acetaldehyde through dehydrogenation:

$$C_2H_5OH \rightarrow C_2H_4 + H_2O$$

$$2C_2H_5OH \rightarrow C_2H_5OC_2H_5 + H_2O$$

$$C_2H_5OH \rightarrow CH_3CHO + H_2$$

In the low-temperature region, the formation of diethyl ether is associated with the contribution of intermolecular dehydration involving the adsorption of two ethanol molecules at two acid sites or their successive adsorption at a single acid site. As the temperature increases, intramolecular dehydration becomes relatively more favourable, and ethylene becomes the principal product. This transition was particularly evident for the Cu-FAU sample.

At 350 °C, Cu-FAU exhibited an ethylene selectivity of 76%. Acetaldehyde selectivity was 11%, while the combined proportion of other products was 13% on a carbon-balance basis. The other-products category included diethyl ether and small amounts of secondary products. This product distribution indicates that Cu-FAU selectively favoured ethanol dehydration.

For Cr-FAU at the same temperature, acetaldehyde selectivity reached 63%, while ethylene selectivity was 18%. Other products accounted for 19%. Thus, the incorporation of Cr^{3+} ions shifted the principal reaction pathway from dehydration towards dehydrogenation.

Table 10. Product selectivity and calculated yields over the Cu-FAU and Cr-FAU catalysts at 350 °C

Sample	Ethylene selectivity (%)	Acetaldehyde selectivity (%)	Other products (%)	Ethylene yield (%)	Acetaldehyde yield (%)
Cu-FAU	76	11	13	69.2	10.0
Cr-FAU	18	63	19	14.2	49.8

The ethylene and acetaldehyde yields were calculated from the product of conversion and the corresponding selectivity. Minor differences in the final values may result from rounding.

The calculated ethylene yield over Cu-FAU at 350 °C was approximately 69.2%. For Cr-FAU, the acetaldehyde yield was approximately 49.8%. These results demonstrate that changing the metal cation substantially affected not only the overall conversion of ethanol but also the product pathway followed by the reaction.

Structure–Acidity–Selectivity Relationship

The high ethylene selectivity observed over Cu-FAU may be associated with the coordination of the hydroxyl oxygen of ethanol to Cu-containing Lewis acid sites. This interaction facilitates C–O bond polarisation and subsequent water elimination, thereby promoting ethylene formation. However, the available catalytic and spectroscopic data do not allow the specific elementary mechanism or rate-determining step to be identified unambiguously. The predominance of acetaldehyde over Cr-FAU is associated with the ability of Cr-containing sites to promote ethanol dehydrogenation. The Lewis/Brønsted ratio of 1.96 determined by Py-FTIR and the broad acid-strength distribution identified by NH_3-TPD indicate that Cr-FAU possesses an active-site environment different from that of Cu-FAU. However, changes in the oxidation states of the Cr species during the reaction and the precise redox mechanism can only be confirmed by XPS, electron paramagnetic resonance, operando spectroscopy or quantitative analysis of hydrogen in the product gas [40].

Textural properties should also be considered when interpreting the catalytic results. Cr-FAU had the lowest BET surface area and micropore volume, at 628 $m^2\ g^{-1}$ and 0.221 $cm^3\ g^{-1}$, respectively. The corresponding values for Cu-FAU were 654 $m^2\ g^{-1}$ and 0.236 $cm^3\ g^{-1}$. The relatively low pore accessibility of Cr-FAU may restrict the transport of ethanol to internal active sites to some extent. Nevertheless, the retention of a highly microporous character in both metal-exchanged samples indicates that a favourable environment for transporting reactant and product molecules through the FAU pore system was preserved.

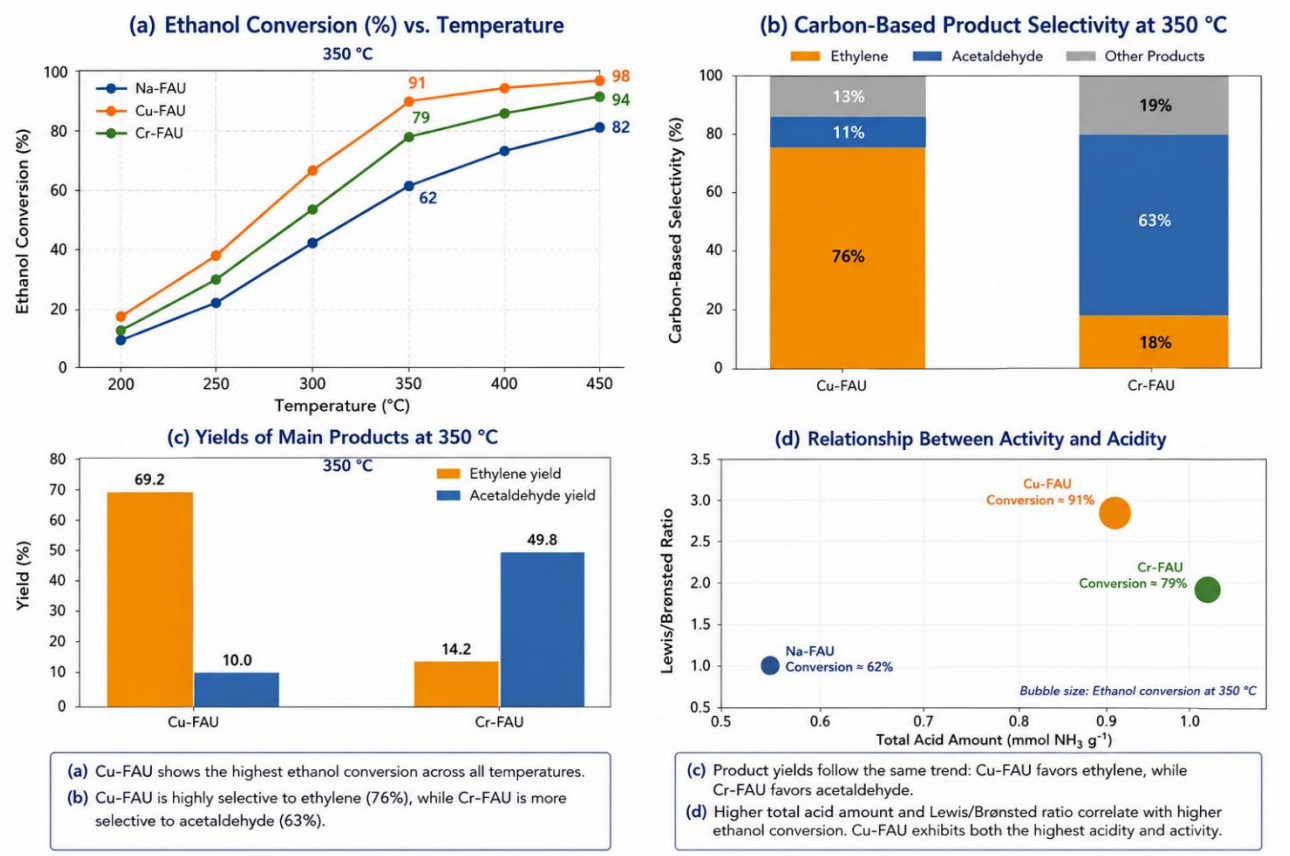


Figure 8. Catalytic performance of the Na-FAU, Cu-FAU and Cr-FAU catalysts in ethanol conversion: (a) dependence of ethanol conversion on reaction temperature; (b) carbon-based selectivity towards the principal products at 350 °C; (c) comparison of ethylene and acetaldehyde yields at 350 °C; (d) relationship between the acidic properties of the catalysts and the principal product pathway. Reaction conditions: WHSV = 2.0 g $_{EtOH}$ g $^{-1}_{catalyst}$ h^{-1}, N_2 carrier gas.

Overall, the catalytic results show that ion exchange with Cu^{2+} and Cr^{3+} created different active-site environments within the FAU zeolite. Cu-FAU exhibited the highest ethanol conversion and ethylene selectivity, making it the more favourable catalyst for the dehydration reaction. Cr-FAU showed a greater tendency towards dehydrogenation, with acetaldehyde predominating in the product distribution. Compared with Na-FAU, the higher activity and distinct selectivity of both metal-exchanged samples indicate that catalytic behaviour was governed more strongly by the interplay among the nature of the acid sites, the properties of the metal cations and pore accessibility than by surface area alone.

4.9. Catalytic Stability and Reusability

The long-term operational stability of the Na-FAU, Cu-FAU and Cr-FAU catalysts was evaluated at 350 °C, using a weight hourly space velocity of 2.0 g $_{EtOH}$ g $^{-1}_{catalyst}$ h^{-1} and N_2 as the carrier gas. During the stability tests, ethanol conversion and selectivity towards the principal products were

monitored at specified time intervals over 24 hours. In addition, five consecutive reaction–regeneration cycles were performed to evaluate the reusability of the metal-exchanged catalysts.

Long-Term Catalytic Stability

Over Na-FAU, the initial ethanol conversion of 62% decreased to 54% by the end of the 24-hour test. This change corresponds to a relative activity loss of approximately 12.9% compared with the initial conversion. The decline in activity may be associated with the gradual accumulation of carbonaceous species adsorbed at weak and medium-strength acid sites, as well as the partial blockage of accessible active sites.

Cu-FAU exhibited higher initial activity together with better long-term stability. Ethanol conversion decreased from 91% at the beginning of the test to 88% after 24 hours. This change represented only 3 percentage points or a relative activity loss of approximately 3.3%. During the test, ethylene selectivity decreased slightly from 76% to 74%. Thus, Cu-FAU largely retained both its high conversion and its selectivity towards ethylene, the dehydration product.

For Cr-FAU, ethanol conversion decreased from 79% to 75% over 24 hours. The relative activity loss was approximately 5.1%. Acetaldehyde selectivity decreased from an initial value of 63% to 60% by the end of the test. This result indicates that the Cr-containing catalyst largely retained its preference for the dehydrogenation pathway under long-term reaction conditions.

Table 11. Results of the 24-hour stability test of the catalysts at 350 °C

Sample	**Initial conversion (%)**	**Conversion after 24 h (%)**	**Absolute decrease (percentage points)**	**Relative activity loss (%)**	**Principal product**	**Initial/final selectivity (%)**
Na-FAU	62	54	8	12.9	Ethylene and other dehydration products	—
Cu-FAU	91	88	3	3.3	Ethylene	76/74
Cr-FAU	79	75	4	5.1	Acetaldehyde	63/60

The relative activity loss was calculated using the following expression:

$$\text{Relative activity loss}(\%) = \frac{X_0 - X_t}{X_0} \times 100$$

where X_0 is the initial ethanol conversion and X_t is the conversion recorded after a specified reaction time. Based on the results obtained, catalytic stability followed the order:

$$\text{Cu-FAU} > \text{Cr-FAU} > \text{Na-FAU}$$

The higher stability of Cu-FAU may be associated with the predominance of strong and accessible Lewis acid sites. The relative Lewis/Brønsted intensity ratio determined by Py-FTIR for Cu-FAU was 2.82, while the LT/HT peak-area ratio obtained by NH_3-TPD was 0.80. These values indicate a substantial proportion of strong sites capable of retaining ammonia up to high temperatures. Moreover, the predominance of ethylene formation during dehydration over Cu-FAU may limit the formation of heavier oxygenated intermediates and carbonaceous deposits.

The slightly greater activity loss of Cr-FAU compared with Cu-FAU may be associated with its lower micropore volume and the ability of acetaldehyde to undergo subsequent condensation reactions. Acetaldehyde may undergo aldol condensation and subsequent oligomerisation at acid sites, producing heavier surface species. The accumulation of such species within the pores may partially reduce the accessibility of the active sites. However, direct confirmation of this mechanism would require thermogravimetric and spectroscopic analyses of the spent catalysts [41].

Reusability and Regeneration

The reusability of the catalysts was evaluated over five consecutive cycles conducted under identical reaction conditions. After each cycle, the catalyst was removed from the reactor, dried under N_2 flow to remove adsorbed organic species and subsequently regenerated in air at 500 °C for 3 hours. The regenerated catalyst was tested in the following cycle using the same catalyst mass and reaction conditions. For Cu-FAU, ethanol conversion was 91% in the first cycle and 87% in the fifth cycle. Ethylene selectivity was 76% and 73%, respectively. The retention of approximately 95.6% of the initial conversion after five cycles indicates that Cu-FAU is a regenerable catalyst.

For Cr-FAU, ethanol conversion decreased from 79% in the first cycle to 74% in the fifth cycle. Acetaldehyde selectivity decreased from 63% to 59%. Approximately 93.7% of the initial activity was retained in the fifth cycle. The relatively greater decrease observed for Cr-FAU may be associated with the more persistent accumulation of carbonaceous residues within the pores or partial changes in local Cr-containing sites during regeneration.

Table 12. Reusability results of the Cu-FAU and Cr-FAU catalysts

Cycle	Cu-FAU conversion (%)	Cu-FAU ethylene selectivity (%)	Cr-FAU conversion (%)	Cr-FAU acetaldehyde selectivity (%)
1	91	76	79	63
2	90	76	78	62
3	89	75	77	61
4	88	74	75	60
5	87	73	74	59

The activity retention after five cycles was calculated using the following expression:

$$\text{Activity retention}(\%) = \frac{X_{\text{final}}}{X_{\text{first}}} \times 100$$

where X_{first} and X_{final} are the ethanol conversions recorded in the first and final reuse cycles, respectively. Based on the calculations, the activity retention values for Cu-FAU and Cr-FAU were 95.6% and 93.7%, respectively.

It is particularly important that the catalysts retained their principal product pathways throughout all cycles. After each regeneration cycle, Cu-FAU maintained an ethylene-dominated product distribution, while Cr-FAU retained its selectivity towards acetaldehyde. This result indicates that the Cu- and Cr-containing active sites were not completely lost during the reaction–regeneration cycles. However, catalytic performance data alone cannot conclusively confirm that the metal cations did not leach, migrate or aggregate.

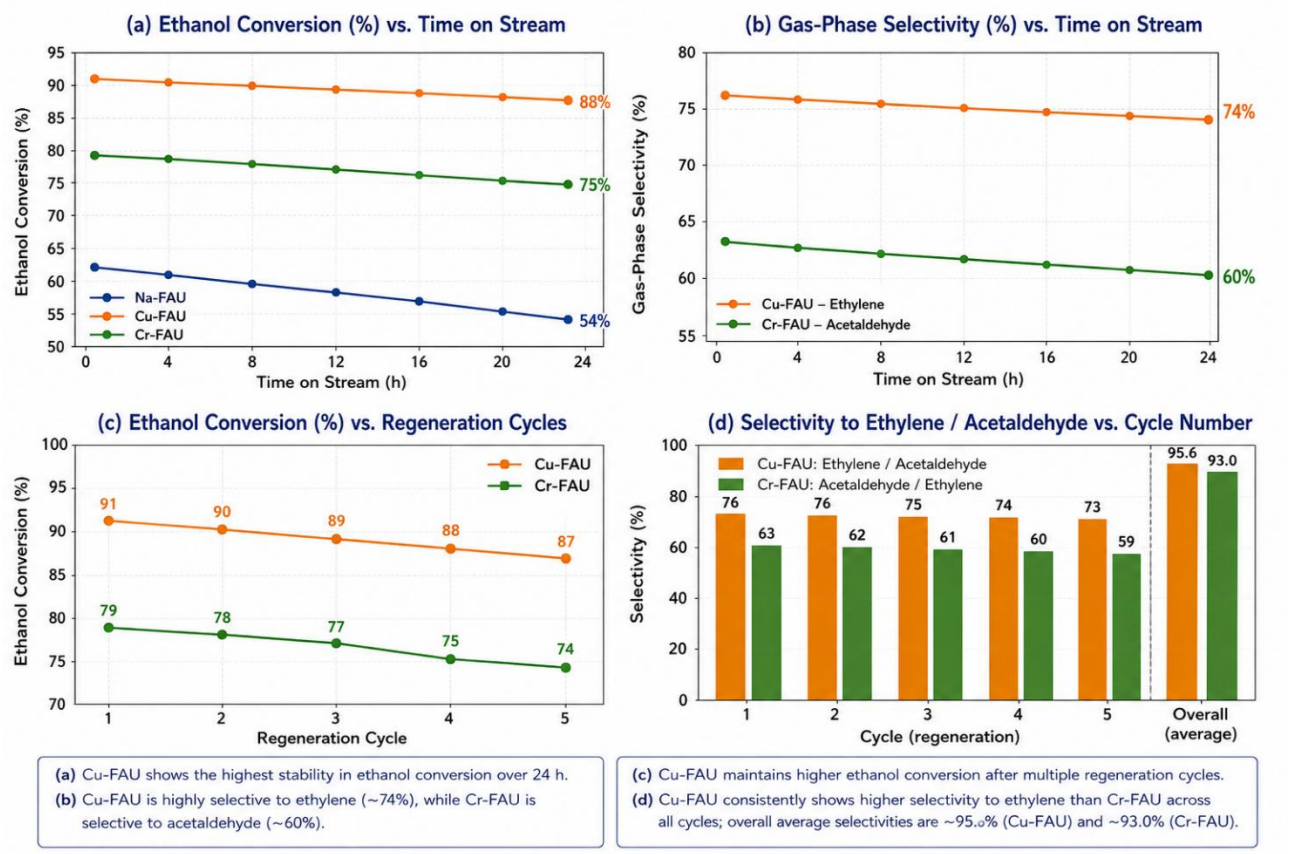


Figure 9. Stability and reusability of the Na-FAU, Cu-FAU and Cr-FAU catalysts: (a) variation in ethanol conversion over 24 hours at 350 °C; (b) dependence of ethylene selectivity for Cu-FAU and acetaldehyde selectivity for Cr-FAU on reaction time; (c) ethanol conversion over five reaction–regeneration cycles; (d) comparison of principal product selectivity during each cycle and activity retention after the fifth cycle. Reaction conditions: 350 °C, WHSV = 2.0 $g_{EtOH}\, g_{catalyst}^{-1}\, h^{-1}$ *and N_2 carrier gas; regeneration conditions: 500 °C in air for 3 hours.*

The combined evaluation of the long-term stability and reusability results with the preceding characterisation data indicates that Cu-FAU possessed a more favourable combination of catalytic properties. Cu-FAU combined high ethanol conversion and ethylene selectivity with a low deactivation rate. Although Cr-FAU was promising for the selective production of acetaldehyde, slightly greater decreases in its activity and selectivity were observed than for Cu-FAU.

Overall, both metal-exchanged FAU catalysts retained most of their catalytic performance during the 24-hour test and five reuse cycles. Cu-FAU demonstrated reusability for the selective dehydration of ethanol to ethylene, while Cr-FAU showed reusability for its dehydrogenation to acetaldehyde. Post-reaction PXRD, N_2 physisorption, SEM–EDS, XPS and TGA analyses are required to determine the catalyst deactivation mechanisms, the stability of the metal species and the amount of carbonaceous deposits more accurately.

4.10. Structure–Acidity–Catalytic Performance Relationship

The combined evaluation of the structural, chemical-composition, textural, acidity and catalytic results obtained for the Na-FAU, Cu-FAU and Cr-FAU samples indicates a direct relationship between the nature of the exchanged cation and catalytic behaviour. According to the PXRD, FTIR, MAS NMR and SEM results, the incorporation of Cu^{2+} and Cr^{3+} ions did not noticeably alter the principal crystalline and aluminosilicate framework structures of the FAU zeolite. Therefore, the catalytic differences observed among the metal-exchanged samples are associated not with framework collapse but mainly with changes in the extra-framework cation composition, the nature of the acid sites and pore accessibility.

Retention of the Framework Structure

The Si/Al molar ratios of 2.50, 2.48 and 2.47 for Na-FAU, Cu-FAU and Cr-FAU, respectively, indicate that the ion-exchange and subsequent thermal treatment stages did not cause substantial changes in the overall chemical composition of the framework. This result is consistent with the retention of the reflections associated with the FAU phase in the PXRD patterns and the absence of reflections attributable to separate crystalline CuO or Cr_2O_3 phases.

The retention of the band at 565–580 cm^{-1}, corresponding to the double six-membered-ring units of the FAU framework, together with the principal T–O–T vibrational bands in the FTIR spectra of all samples, confirmed the integrity of the aluminosilicate framework. The presence of the dominant tetrahedral Al(IV) resonance at 58–62 ppm in the solid-state ^{27}Al MAS NMR spectra indicated that most of the aluminium atoms remained within the framework. The weak Al(VI) contribution observed near 0 ppm in Cr-FAU suggested only the possible formation of trace amounts of extra-framework aluminium and did not confirm extensive dealumination.

The similar positions of the $Q^4(nAl)$ resonances and overall spectral envelopes in the ^{29}Si MAS NMR spectra showed that the local coordination environment of silicon was also largely preserved. The retention of octahedral and truncated-octahedral crystals in the SEM images supported these findings at the particle level. Thus, the overall structural analyses indicate that metal exchange of the FAU—

Structure–Acidity–Catalytic Performance Relationship

The combined analysis of the results obtained for the Na-FAU, Cu-FAU and Cr-FAU samples shows that catalytic behaviour did not depend on a single parameter, such as metal content or total acidity. Ethanol conversion and product selectivity were determined by the interplay among framework retention, pore accessibility, degree of ion exchange, the nature and strength of the acid sites, and the chemical properties of the exchanged metal cation.

Structural Integrity and Pore Accessibility

The PXRD results showed that the FAU crystalline phase was largely retained after ion exchange with Cu^{2+} and Cr^{3+} and that no separate crystalline CuO or Cr_2O_3 phases formed within the detection limit. This result was supported by the retention of the octahedral and truncated-octahedral crystal morphology in the SEM images. The broad distribution of the Cu and Cr signals throughout the selected crystals in the EDS maps indicated that no large, micrometre-scale metal-rich aggregates had formed.

The retention of the principal framework vibrations associated with the FAU topology in the FTIR spectra, including the band at 565–580 cm^{-1} related to double six-membered-ring units, confirmed that the aluminosilicate framework remained intact after ion exchange. The predominance of the tetrahedral Al(IV) resonance at 58–62 ppm in the solid-state ^{27}Al MAS NMR spectra indicated that extensive dealumination had not occurred. The weak signal observed near 0 ppm in Cr-FAU was consistent only with the possible presence of trace amounts of extra-framework Al(VI) species. The similar Q^4(nAl) envelopes in the ^{29}Si MAS NMR spectra also indicated that the local silicon environment remained largely unchanged.

These findings are consistent with the Si/Al molar ratios determined by XRF. The Si/Al ratios were 2.50, 2.48 and 2.47 for Na-FAU, Cu-FAU and Cr-FAU, respectively. Therefore, the differences in catalytic performance cannot be explained by substantial changes in the chemical composition of the framework or in the FAU topology. The principal changes occurred in the extra-framework cation composition, pore accessibility and acid-site distribution.

According to the N_2 physisorption results, the specific surface area and micropore volume decreased to some extent after ion exchange. The BET surface area decreased from 721 $m^2\ g^{-1}$ for Na-FAU to 654 $m^2\ g^{-1}$ for Cu-FAU and 628 $m^2\ g^{-1}$ for Cr-FAU. The corresponding micropore volumes were 0.268, 0.236 and 0.221 $cm^3\ g^{-1}$. Nevertheless, the retention of the Type I character of the isotherms and the dominant micropore region indicated that the FAU pore system had not collapsed.

The decrease in pore accessibility may be associated with the location of metal cations at intracrystalline sites and pore entrances. Despite this reduction, Cu-FAU and Cr-FAU exhibited higher catalytic activity than Na-FAU, although they had lower surface areas. This result demonstrates that ethanol conversion was not governed solely by the total surface area [42].

Effect of the Degree of Ion Exchange on Active-Site Formation

The sodium content decreased from 5.17 mmol g^{-1} in the original Na-FAU sample to 1.35 mmol g^{-1} in Cu-FAU and 3.00 mmol g^{-1} in Cr-FAU. The degrees of ion exchange calculated from the residual Na contents were 74% for Cu-FAU and 42% for Cr-FAU. Taking charge equivalence into account, the metal contents corresponding to the amount of replaced Na^+ were 1.91 mmol Cu g^{-1} for Cu-FAU and 0.72 mmol Cr g^{-1} for Cr-FAU.

The higher degree of ion exchange in Cu-FAU favoured the formation of a greater number of extra-framework Cu-containing sites. In Cr-FAU, the retention of a greater amount of residual Na^+ and the lower number of Cr^{3+} ions required to maintain the charge balance resulted in a different active-site density and local coordination environment.

However, the degree of ion exchange alone does not explain the catalytic results. The charge, polarising ability and hydration of the metal cation, its interaction with framework oxygen atoms and possible changes in its electronic structure during the reaction also determine the function of the active sites.

Nature of the Acid Sites and Catalytic Activity

The Py-FTIR results showed that ion exchange substantially altered the relative distribution of Brønsted and Lewis acid sites. When normalised to the values for Na-FAU, the relative intensity of the Lewis band at 1450 cm^{-1} increased to 1.72 for Cu-FAU, while the intensity of the Brønsted band at 1545 cm^{-1} decreased to 0.61. Consequently, the relative Lewis/Brønsted ratio was 2.82. The corresponding values for Cr-FAU were 1.55, 0.79 and 1.96.

These results indicate a stronger predominance of Lewis-acidic sites in Cu-FAU, whereas the Lewis and Brønsted contributions remained relatively more balanced in Cr-FAU. The normalised Py-FTIR values should be interpreted as relative changes among the samples rather than as absolute acid-site concentrations.

The NH_3-TPD results showed that the total acidity was 0.58 mmol NH_3 g^{-1} for Na-FAU, 0.84 mmol NH_3 g^{-1} for Cu-FAU and 0.91 mmol NH_3 g^{-1} for Cr-FAU. Thus, total acidity followed the order:

$$\text{Cr-FAU} > \text{Cu-FAU} > \text{Na-FAU}$$

However, the order of catalytic activity at 350 °C was different:

$$\text{Cu-FAU} > \text{Cr-FAU} > \text{Na-FAU}$$

This difference shows that total acidity was not the only parameter determining catalytic activity. In the NH_3-TPD profile of Cu-FAU, the high-temperature maximum shifted to 447 °C, while the LT/HT peak-area ratio decreased to 0.80. This change corresponds to an increase in the relative proportion of sites that retained ammonia more strongly. For Cr-FAU, the high-temperature maximum was 438 °C and the LT/HT ratio was 1.10. Therefore, although Cr-FAU had the highest total NH_3 uptake, Cu-FAU exhibited an acid-site nature and strength distribution more favourable for ethanol conversion.

Development of Catalytic Activity

At 350 °C, ethanol conversion was 62% for Na-FAU, 91% for Cu-FAU and 79% for Cr-FAU. At 450 °C, the conversions over Cu-FAU and Cr-FAU reached 98% and 94%, respectively. Although Cu-FAU had a lower BET surface area than Na-FAU, it exhibited higher conversion, demonstrating the high effectiveness of the Cu-containing active sites.

The high activity of Cu-FAU may be explained by the combined effects of the following factors:

1. A higher degree of ion exchange of 74%;
2. A higher Cu content based on charge balance;
3. Strong Lewis character identified by Py-FTIR;
4. An increased relative proportion of high-temperature sites in the NH_3-TPD profile;
5. The retention of a sufficiently high surface area and micropore volume for transporting ethanol to the active sites.

Although Cr-FAU had a higher total acidity, its lower degree of ion exchange, reduced pore accessibility and broader acid-strength distribution may have caused its conversion to remain below that of Cu-FAU. Furthermore, the tendency of the Cr-containing sites to direct the reaction towards acetaldehyde formation affected both the overall conversion and product distribution.

Nature of the Acid Sites and Product Selectivity

At 350 °C, Cu-FAU exhibited selectivities of 76% towards ethylene and 11% towards acetaldehyde. For Cr-FAU, acetaldehyde selectivity was 63%, whereas ethylene selectivity was only 18%. The calculated product yields were 69.2% ethylene for Cu-FAU and 49.8% acetaldehyde for Cr-FAU.

The predominance of ethylene over Cu-FAU is associated with the interaction of coordinatively unsaturated Cu-containing Lewis sites with the hydroxyl oxygen of ethanol. This coordination may facilitate the polarisation of the ethanol molecule and its dehydration through water elimination:

$$C_2H_5OH \rightarrow C_2H_4 + H_2O$$

The predominance of acetaldehyde over Cr-FAU is associated with the greater tendency of Cr-containing sites to promote ethanol dehydrogenation:

$$C_2H_5OH \rightarrow CH_3CHO + H_2$$

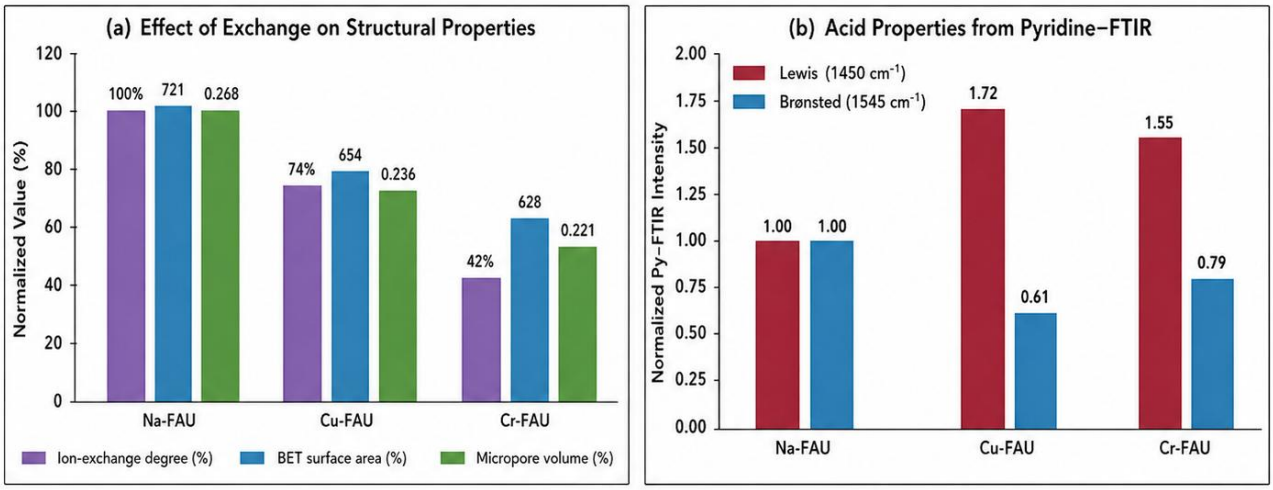
These results show that changing the metal cation can selectively regulate the principal reaction pathway within the same FAU framework. Cu^{2+} mainly promoted the acid-catalysed dehydration pathway, whereas the Cr-containing sites enhanced dehydrogenation. However, additional studies involving operando spectroscopy, isotope labelling and hydrogen balance measurements are required to confirm the precise elementary reaction steps and the redox role of the Cr species.

Table 13. Summary comparison of the structural, textural, acidity and catalytic parameters

Parameter	**Na-FAU**	**Cu-FAU**	**Cr-FAU**
Si/Al molar ratio	2.50	2.48	2.47
Residual Na (mmol g^{-1})	5.17	1.35	3.00

Degree of ion exchange (%)	—	74	42
Metal content based on charge balance (mmol g^{-1})	—	1.91 Cu	0.72 Cr
BET surface area (m^2 g^{-1})	721	654	628
Micropore volume (cm^3 g^{-1})	0.268	0.236	0.221
Relative Lewis intensity determined by Py-FTIR	1.00	1.72	1.55
Relative Brønsted intensity determined by Py-FTIR	1.00	0.61	0.79
Relative Lewis/Brønsted ratio	1.00	2.82	1.96
Total acidity (mmol NH_3 g^{-1})	0.58	0.84	0.91
LT/HT peak-area ratio	1.40	0.80	1.10
Ethanol conversion at 350 °C (%)	62	91	79
Principal product at 350 °C	Mixed products	Ethylene	Acetaldehyde
Principal-product selectivity (%)	—	76	63
Principal-product yield (%)	—	69.2	49.8

The results in Table 13 demonstrate three principal relationships. First, the retention of the Si/Al ratio and FAU topology indicates that the catalytic differences were not associated with extensive changes in the framework. Second, the increase in catalytic activity despite the reduction in surface area confirms that the quality and chemical nature of the active sites were more important than the total surface area. Third, the absence of a direct linear relationship between total acidity and conversion indicates that product formation depended not only on the number of acid sites but also on their type and strength.



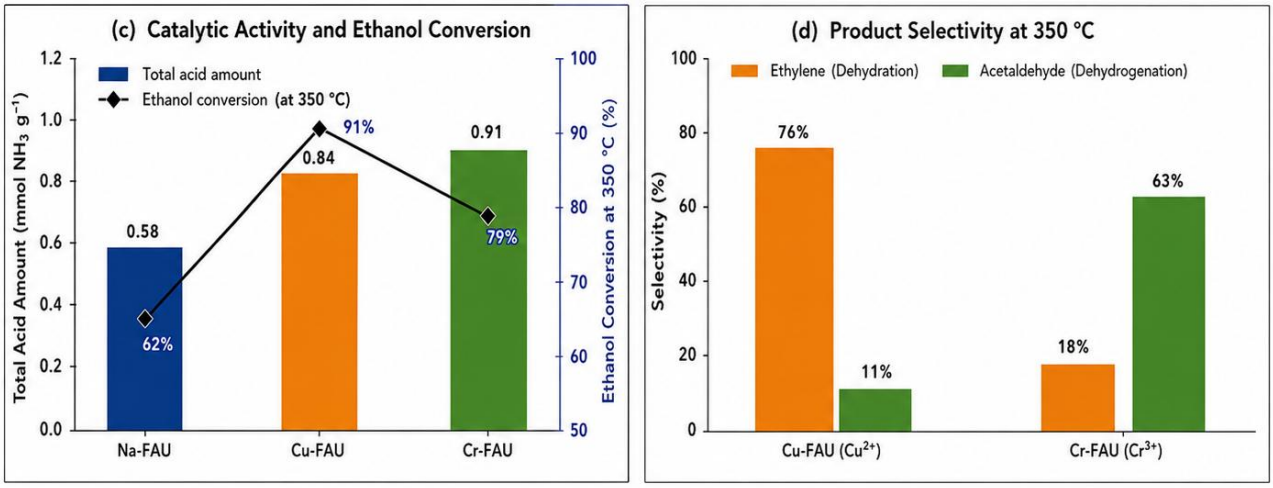


Figure 10. Structure–acidity–catalytic performance relationship in the Na-FAU, Cu-FAU and Cr-FAU samples: (a) comparison of the degree of ion exchange, BET surface area and micropore volume; (b) normalised Lewis and Brønsted acid sites determined by Py-FTIR; (c) total acidity and ethanol conversion at 350 °C; (d) comparison of the dehydration and dehydrogenation pathways as a function of the nature of the metal cation.

Overall, Cu-FAU combined a high degree of ion exchange, an accessible microporous structure and strong Lewis-acidic sites, creating the most favourable catalytic environment for converting ethanol to ethylene. Although Cr-FAU had a higher total acidity, the different chemical nature of its active sites directed the reaction mainly towards acetaldehyde formation. Despite its higher surface area, Na-FAU exhibited lower acidity and catalytic activity than the metal-exchanged samples. Therefore, the targeted regulation of catalytic behaviour in FAU-based catalysts requires the combined optimisation of not only the surface area and total number of acid sites but also the nature of the extra-framework cation, the degree of exchange, the type of acid sites and their accessibility within the pores [43, 44].

5. Conclusion

In this study, the structural, textural, acidic and catalytic properties of Cu-FAU and Cr-FAU samples prepared by exchanging hydrothermally synthesised Na-FAU zeolite with Cu^{2+} and Cr^{3+} ions were investigated comparatively. The XRD and FTIR results showed that the FAU framework was largely retained after ion exchange. At the same time, the changes observed in diffraction intensity, vibrational bands and pore parameters confirmed the interaction of the Cu and Cr species with the zeolite structure. SEM–EDS analysis showed that the metal species were distributed throughout the catalyst particles, while the N_2 adsorption–desorption results revealed that ion exchange affected the specific surface area and pore volume to some extent.

According to the NH_3-TPD results, the total acidity was 0.58 mmol NH_3 g^{-1} for Na-FAU, 0.84 mmol NH_3 g^{-1} for Cu-FAU and 0.91 mmol NH_3 g^{-1} for Cr-FAU. Thus, total acidity increased in the order

Cr-FAU > Cu-FAU > Na-FAU. This finding indicates that the incorporation of transition-metal ions resulted in the formation of new Lewis acid sites and altered the strength distribution of the existing acid sites. However, the catalytic activity observed at 350 °C did not follow the same order as total acidity. This discrepancy showed that ethanol conversion depended not only on the number of acid sites but also on their strength, type, location within the pores and accessibility to the reactants.

Among the samples compared, Cu-FAU exhibited a more favourable balance among acidity, metal dispersion and pore accessibility. The dehydrogenation sites created by the Cu species affected the ethanol conversion rate and product distribution, while the acid sites of the FAU framework determined the direction of the parallel dehydration reaction. Although Cr-FAU had the highest total acidity, the absence of a proportional increase in its catalytic performance may be associated with the location of some Cr species at less accessible sites, their strong adsorption or their restriction of diffusion within the pores. Na-FAU exhibited weaker acidic and redox functionality than the metal-exchanged samples.

The principal scientific contribution of this study is the determination, through a unified comparative approach, of the effects of Na^{+}, Cu^{2+} and Cr^{3+} cations on the structure–acidity–activity relationship within the same FAU framework. The findings demonstrate that evaluating the catalytic behaviour of metal-exchanged zeolites solely on the basis of metal content or total acidity is insufficient. The coordination state and dispersion of the metal species, the strength distribution of the acid sites and the preservation of the pore system must be considered together. From this perspective, Cu-FAU was identified as the more promising catalytic system for the targeted conversion of ethanol.

Future studies should determine the oxidation and coordination states of the Cu and Cr species using *in situ* XPS, XAS or solid-state NMR, separately quantify the Brønsted and Lewis acid sites, and investigate long-term catalytic stability. Optimising the metal loading and ion-exchange conditions may increase the accessibility of active sites in FAU-based catalysts, limit side reactions and improve selectivity towards the desired product.

Funding

The authors declare that no funding was received for the research, authorship, and/or publication of this article.

References

[1] H. Xiang, R. Xin, N. Prasongthum, P. Natewong, T. Sooknoi, J. Wang, P. Reubroycharoen, X. Fan, Catalytic conversion of bioethanol to value-added chemicals and fuels: A review, Resour. Chem. Mater. 1 (2022) 47–68. https://doi.org/10.1016/j.recm.2021.12.002.

[2] H. Ma, S. Zhang, H. Gao, D. Wen, Metal-modified zeolites for catalytic dehydration of bioethanol to ethylene: Mechanisms, preparation, and performance, Catalysts 15 (2025) 791. https://doi.org/10.3390/catal15080791.

[3] M. Ngcobo, P.R. Makgwane, M.K. Mathe, A minireview on solid acid catalysts for dehydration of bioethanol to renewable ethylene: An update on catalysts development progress, Appl. Catal. O Open 193 (2024) 206976. https://doi.org/10.1016/j.apcato.2024.206976.

[4] C.-Y. Wu, H.-S. Wu, Ethylene formation from ethanol dehydration using ZSM-5 catalyst, ACS Omega 2 (2017) 4287–4296. https://doi.org/10.1021/acsomega.7b00680.

[5] X. Zhou, C. Wang, Y. Chu, J. Xu, Q. Wang, G. Qi, X. Zhao, N. Feng, F. Deng, Observation of an oxonium ion intermediate in ethanol dehydration to ethene on zeolite, Nat. Commun. 10 (2019) 1961. https://doi.org/10.1038/s41467-019-09956-7.

[6] M. Hu, Y. Chu, C. Wang, W. Cai, Q. Wang, J. Xu, F. Deng, Unveiling the thermodynamic–kinetic trade-off effect on acid sites in zeolite-catalyzed alcohol dehydration, Nat. Commun. 17 (2026) 3675. https://doi.org/10.1038/s41467-026-70418-y.

[7] L. Chen, B. Xu, S. Wang, S. Ren, F. Yang, W. Zhang, Y. Lan, C. Chen, J. Li, Y. Su, Advancements in synthesis strategies and environmental application of FAU-type zeolite: Bibliometric-driven review, Green Energy Environ. 11 (2026) 36–61. https://doi.org/10.1016/j.gee.2025.10.003.

[8] K. Kvande, S. Prodinger, F. Schlimpen, P. Beato, P. Pale, S. Chassaing, S. Svelle, Copper-zeolites prepared by solid-state ion exchange—Characterization and evaluation for the direct conversion of methane to methanol, Top. Catal. 66 (2023) 1406–1417. https://doi.org/10.1007/s11244-022-01763-7.

[9] D. Yu, W. Dai, G. Wu, N. Guan, L. Li, Stabilizing copper species using zeolite for ethanol catalytic dehydrogenation to acetaldehyde, Chin. J. Catal. 40 (2019) 1375–1384. https://doi.org/10.1016/S1872-2067(19)63378-4.

[10] J.E. Schmidt, R. Oord, W. Guo, J.D. Poplawsky, B.M. Weckhuysen, Nanoscale tomography reveals the deactivation of automotive copper-exchanged zeolite catalysts, Nat. Commun. 8 (2017) 1666. https://doi.org/10.1038/s41467-017-01765-0.

[11] P. Xiao, Y. Wang, L. Wang, H. Toyoda, K. Nakamura, S. Bekhti, Y. Lu, J. Huang, H. Gies, T. Yokoi, Understanding the effect of spatially separated Cu and acid sites in zeolite catalysts on oxidation of methane, Nat. Commun. 15 (2024) 2718. https://doi.org/10.1038/s41467-024-46924-2.

[12] F. Ayari, M. Mhamdi, T. Hammedi, J. Álvarez-Rodríguez, A. Guerrero-Ruiz, G. Delahay, A. Ghorbel, Influence of the parent zeolite structure on chromium speciation and catalytic properties of Cr-zeolite catalysts in the ethylene ammoxidation, Appl. Catal. A Gen. 439–440 (2012) 88–100. https://doi.org/10.1016/j.apcata.2012.06.037.

[13] H. Zhu, X. Bao, The principle of metal-zeolite catalyzing alkane dehydrogenation, Natl. Sci. Rev. 12 (2025) nwaf446. https://doi.org/10.1093/nsr/nwaf446.

[14] M.B. Park, E.D. Park, W.-S. Ahn, Recent progress in direct conversion of methane to methanol over copper-exchanged zeolites, Front. Chem. 7 (2019) 514. https://doi.org/10.3389/fchem.2019.00514.

[15] Y. Yuan, Z. Zhao, R.F. Lobo, B. Xu, Site diversity and mechanism of metal-exchanged zeolite catalyzed non-oxidative propane dehydrogenation, Adv. Sci. 10 (2023) 2207756. https://doi.org/10.1002/advs.202207756.

[16] D. Verboekend, N. Nuttens, R. Locus, J. Van Aelst, P. Verolme, J.C. Groen, J. Pérez-Ramírez, B.F. Sels, Synthesis, characterisation, and catalytic evaluation of hierarchical faujasite zeolites: Milestones, challenges, and future directions, Chem. Soc. Rev. 45 (2016) 3331–3352. https://doi.org/10.1039/C5CS00520E.

[17] Y.-G. Chen, W. Sofińska-Chmiel, G.-Y. Lv, D. Kołodyńska, S.-H. Chen, Application of modern research methods for the physicochemical characterization of ion exchangers, Materials 14 (2021) 7067. https://doi.org/10.3390/ma14227067.

[18] A. Ahmadon, L.S. Mohd Nazir, Y.F. Yeong, S. Sabdin, Formation of pure NaX zeolite: Effect of ageing and hydrothermal synthesis parameters, IOP Conf. Ser. Mater. Sci. Eng. 458 (2018) 012002. https://doi.org/10.1088/1757-899X/458/1/012002.

[19] L. Guan, Z. Wang, D. Lu, Evolution of zeolite crystals in self-supporting faujasite blocks: Effects of hydrothermal conditions, Materials 12 (2019) 1965. https://doi.org/10.3390/ma12121965.

[20] Z. Tahraoui, H. Nouali, C. Marichal, P. Forler, J. Klein, T.J. Daou, Influence of the compensating cation nature on the water adsorption properties of zeolites, Molecules 25 (2020) 944. https://doi.org/10.3390/molecules25040944.

[21] A. Gęsikiewicz-Puchalska, M. Zgrzebnicki, B. Michalkiewicz, A. Kałamaga, U. Narkiewicz, A.W. Morawski, R. Wrobel, Changes in porous parameters of the ion exchanged X zeolite and their effect on CO_2 adsorption, Molecules 26 (2021) 7520. https://doi.org/10.3390/molecules26247520.

[22] X. Wang, N.M. Martin, J. Nilsson, S. Carlson, J. Gustafson, M. Skoglundh, P.-A. Carlsson, Copper-modified zeolites and silica for conversion of methane to methanol, Catalysts 8 (2018) 545. https://doi.org/10.3390/catal8110545.

[23] A. Węgrzyniak, S. Jarczewski, A. Węgrzynowicz, B. Michorczyk, P. Kuśtrowski, P. Michorczyk, Catalytic behavior of chromium oxide supported on nanocasting-prepared mesoporous alumina in dehydrogenation of propane, Nanomaterials 7 (2017) 249. https://doi.org/10.3390/nano7090249.

[24] E.V. Golubina, I.Y. Kaplin, A.V. Gorodnova, E.S. Lokteva, O.Y. Isaikina, K.I. Maslakov, Non-oxidative propane dehydrogenation on CrO_x–ZrO_2–SiO_2 catalyst prepared by one-pot template-assisted method, Molecules 27 (2022) 6095. https://doi.org/10.3390/molecules27186095.

[25] J. Jiao, J. Kanellopoulos, W. Wang, S.S. Ray, H. Foerster, D. Freude, M. Hunger, Characterization of framework and extra-framework aluminum species in non-hydrated zeolites Y by ^{27}Al spin-echo, high-speed MAS, and MQMAS NMR spectroscopy at B_0 = 9.4 to 17.6 T, Phys. Chem. Chem. Phys. 7 (2005) 3221–3226. https://doi.org/10.1039/B508358C.

[26] S.R. Batool, V.L. Sushkevich, J.A. van Bokhoven, Factors affecting the generation and catalytic activity of extra-framework aluminum Lewis acid sites in aluminum-exchanged zeolites, ACS Catal. 14 (2024) 678–690. https://doi.org/10.1021/acscatal.3c04195.

[27] N.E. Gordina, T.N. Borisova, K.S. Klyagina, I.A. Astrakhantseva, A.A. Ilyin, R.N. Rumyantsev, Investigation of NH_3 desorption kinetics on the LTA and SOD zeolite membranes, Membranes 12 (2022) 147. https://doi.org/10.3390/membranes12020147.

[28] D.S. Zasukhin, I.A. Kasyanov, Y.G. Kolyagin, A.I. Bulygina, K.C. Kharas, I.I. Ivanova, Evaluation of zeolite acidity by ^{31}P MAS NMR spectroscopy of adsorbed phosphine oxides: Quantitative or not?, ACS Omega 7 (2022) 12318–12328. https://doi.org/10.1021/acsomega.2c00804.

[29] A. Zachariou, A.P. Hawkins, R.F. Howe, J.M.S. Skakle, N. Barrow, P. Collier, D.W. Nye, R.I. Smith, G.B.G. Stenning, S.F. Parker, D. Lennon, Counting the acid sites in a commercial ZSM-5 zeolite catalyst, ACS Phys. Chem. Au 3 (2023) 74–83. https://doi.org/10.1021/acsphyschemau.2c00040.

[30] P. Čičmanec, J. Kotera, J. Vaculík, R. Bulánek, Influence of substrate concentration on kinetic parameters of ethanol dehydration in MFI and CHA zeolites and relation of these kinetic parameters to acid–base properties, Catalysts 12 (2022) 51. https://doi.org/10.3390/catal12010051.

[31] P. Babayeva, A. Heydərov, M.D. Turan, H. Nizamoğlu, T. Demir, Optimization of aluminum leaching from alunite ore with NaOH using response surface methodology (RSM), J. Sustain. Metall. 11 (2025) 2677–2687. https://doi.org/10.1007/s40831-025-01156-6.

[32] P.I. Kyriienko, O.V. Larina, S.O. Soloviev, S.M. Orlyk, C. Calers, S. Dzwigaj, Ethanol conversion into 1,3-butadiene by the Lebedev method over MTaSiBEA zeolites (M = Ag, Cu, Zn), ACS Sustain. Chem. Eng. 5 (2017) 2075–2083. https://doi.org/10.1021/acssuschemeng.6b01728.

[33] P. Xiao, Y. Wang, K. Nakamura, Y. Lu, T. De Baerdemaeker, A.-N. Parvulescu, U. Müller, D. De Vos, X. Meng, F.-S. Xiao, W. Zhang, B. Marler, U. Kolb, R. Osuga, M. Nishibori, H. Gies, T. Yokoi, Highly effective Cu/AEI zeolite catalysts contribute to continuous conversion of methane to methanol, ACS Catal. 13 (2023) 11057–11068. https://doi.org/10.1021/acscatal.3c02271.

[34] S.R. Batool, V.L. Sushkevich, J.A. van Bokhoven, Correlating Lewis acid activity to extra-framework aluminum species in zeolite Y introduced by ion-exchange, J. Catal. 408 (2022) 24–35. https://doi.org/10.1016/j.jcat.2022.02.010.

[35] T.J. Daou, T. Dos Santos, H. Nouali, L. Josien, L. Michelin, L. Pieuchot, P. Dutournie, Synthesis of FAU-type zeolite membranes with antimicrobial activity, Molecules 25 (2020) 3414. https://doi.org/10.3390/molecules25153414.

[36] M.K. Król, P. Jeleń, The effect of heat treatment on the structure of zeolite A, Materials 14 (2021) 4642. https://doi.org/10.3390/ma14164642.

[37] S. Ferdov, Interzeolite transformation from FAU-to-EDI type of zeolite, Molecules 29 (2024) 1744. https://doi.org/10.3390/molecules29081744.

[38] I.V. Joseph, L. Tosheva, G. Miller, A.M. Doyle, FAU-type zeolite synthesis from clays and its use for the simultaneous adsorption of five divalent metals from aqueous solutions, Materials 14 (2021) 3738. https://doi.org/10.3390/ma14133738.

[39] H. Kim, M. Numan, C. Jo, Catalytic dehydration of ethanol over WO_x nanoparticles supported on MFI (Mobile Five) zeolite nanosheets, Catalysts 9 (2019) 670. https://doi.org/10.3390/catal9080670.

[40] R. Larsson, Propane dehydrogenation catalyzed by ZSM-5 zeolites: A mechanistic study based on the selective energy transfer (SET) theory, Molecules 20 (2015) 2529–2535. https://doi.org/10.3390/molecules20022529.

[41] Q. Wang, H. Chen, F. He, Q. Liu, N. Xu, L. Fan, C. Wang, L. Zhang, R. Zhou, High-performance FAU zeolite membranes derived from nano-seeds for gas separation, Membranes 13 (2023) 858. https://doi.org/10.3390/membranes13110858.

[42] M.G. Shelyapina, E.A. Krylova, Y.M. Zhukov, I.A. Zvereva, I. Rodriguez-Iznaga, V. Petranovskii, S. Fuentes-Moyado, Comprehensive analysis of the copper exchange implemented in ammonia and protonated forms of mordenite using microwave and conventional methods, Molecules 24 (2019) 4216. https://doi.org/10.3390/molecules24234216.

[43] M. Smoliło, K. Samson, T. Zhou, D. Duraczyńska, M. Ruggiero-Mikołajczyk, A. Drzewiecka-Matuszek, D. Rutkowska-Zbik, Oxidative dehydrogenation of propane over vanadium-containing faujasite zeolite, Molecules 25 (2020) 1961. https://doi.org/10.3390/molecules25081961.
[44] S.A. Yashnik, T.A. Surovtsova, A.V. Salnikov, V.N. Parmon, Leaching stability and redox activity of copper-MFI zeolites prepared by solid-state transformations: Comparison with ion-exchanged and impregnated samples, Materials 16 (2023) 671. https://doi.org/10.3390/ma16020671.
[45] P.B.F. Sousa, L. Bieseki, S.B.C. Pergher, Seed-assisted crystallization in the hydrothermal synthesis of FAU zeolite from acid-treated residue glass powder, Materials 18 (2025) 1393. https://doi.org/10.3390/ma18071393.